

Photometric scaling relations of lenticular and spiral galaxies

E. Laurikainen^{1*}, H. Salo¹, R. Buta², J. H. Knapen^{3,4} and S. Comerón^{3,4}

¹*Division of Astronomy, Department of Physical Sciences, University of Oulu, FIN-90014, Finland*

²*Department of Physics and Astronomy, University of Alabama, Box 870324, Tuscaloosa, AL 35487*

³*Instituto de Astrofísica de Canarias, E-38200 La Laguna, Tenerife, Spain*

⁴*Departamento de Astrofísica de Canarias, E-38205 La Laguna, Tenerife, Spain*

Accepted: Received:

ABSTRACT

Photometric scaling relations are studied for S0 galaxies and compared with those obtained for spirals. New two-dimensional multi-component decompositions are presented for 122 early-type disk galaxies, using deep K_s -band images. Combining them with our previous decompositions, the final sample consists of 175 galaxies (Near-Infrared Survey of S0s, NIRS0S: 117 S0s + 22 S0/a and 36 Sa galaxies). As a comparison sample we use the Ohio State University Bright Spiral Galaxy Survey (OSUBSGS) of nearly 200 spirals, for which similar multi-component decompositions have previously been made by us. The improved statistics, deep images, and the homogeneous decomposition method used, allows us to re-evaluate the parameters of the bulges and disks. For spirals we largely confirm previous results, which are compared with those obtained for S0s. Our main results are as follows. (1) Important scaling relations are present, indicating that the formative processes of bulges and disks in S0s are coupled (e.g. $M_K^o(disk) = 0.63 M_K^o(bulge) - 9.3$), like has been found previously for spirals (for OSUBSGS spirals $M_K^o(disk) = 0.38 M_K^o(bulge) - 15.5$; the rms deviation from these relations is 0.5 mag, for S0s and spirals). (2) We obtain median $r_{eff}/h_r \sim 0.20, 0.15$ and 0.10 for S0, S0/a-Sa and Sab-Sc galaxies, respectively: these values are smaller than predicted by simulation models in which bulges are formed by galaxy mergers. (3) The properties of bulges of S0s are different from the elliptical galaxies, which is manifested in the $M_K^o(bulge)$ vs r_{eff} relation, in the photometric plane (μ_0, n, r_{eff}), and to some extent also in the Kormendy relation ($\langle \mu \rangle_{eff}$ vs r_{eff}). The bulges of S0s are similar to bulges of spirals with $M_K^o(bulge) < -20$ mag. Some S0s have small bulges, but their properties are not compatible with the idea that they could evolve to dwarfs by galaxy harassment. (4) The relative bulge flux (B/T) for S0s covers the full range found in the Hubble sequence, even with 13% having $B/T < 0.15$, typical for late-type spirals. (5) The values and relations of the parameters of the disks ($h_r^o, M_K^o(disk), \mu_o(0)$) of the S0 galaxies in NIRS0S are similar to those obtained for spirals in the OSUBSGS. Overall, our results support the view that spiral galaxies with bulges brighter than -20 mag in the K -band can evolve directly into S0s, due to stripping of gas followed by truncated star formation.

Key words: galaxies: elliptical and lenticular - galaxies: evolution - galaxies: structure

* E-mail: eija.laurikainen@oulu.fi

1 INTRODUCTION

The position of S0 galaxies between ellipticals and spirals in galaxy classification schemes (Hubble 1926; de Vaucouleurs 1959; Sandage 1961) has made them of particular interest in any scenario of galaxy formation and evolution. Yet the debate on their origin is open. In the current paradigm, the hierarchical Lambda Cold Dark Matter (Λ CDM) cosmology (Somerville & Primack 1999; Steinmetz & Navarro 2002), the disks are formed first by cooling of gas inside rotating dark matter halos, whereas both the elliptical galaxies and the bulges of disk galaxies are suggested to have formed in major or minor mergers, respectively (Khochfar & Silk 2006). The bulges formed in this manner are dynamically hot and their basic properties were established already in the merger process (Khochfar & Burkert 2005), not affected by the subsequently growing disks. Within Λ CDM, S0s are formed in galaxy mergers in a similar manner as the elliptical galaxies, or they are transformed from spirals which have lost their disk gas by some stripping mechanism (Gunn & Gott 1972; Moore et al. 1996; Bekki, Couch & Shioya 2002). Therefore, it is important to study whether the S0 galaxies are more tightly related to ellipticals or to spirals. However, even if the bulges in S0s were found to be similar to those in spirals, this does not yet answer the question of what the formative processes of bulges in S0s are.

It has been suggested that two types of bulges appear: 1) classical merger-built bulges, and 2) disk-like bulges formed by star formation in the disk (Kormendy 1982; see also review by Kormendy & Kennicutt 2004). Boxy/peanut bulges are often listed as a separate class, but as they are assumed to be part of a bar (Athanasoula, Lambert & Dehnen 2005), they are basically disk-related structures. Bulges in late-type spirals are typically photometrically disk-like (Andredakis & Sanders 1994; Carollo et al., 1997, 1998) rotationally supported structures (Cappellari et al. 2007), whereas for the bulges of early-type spirals contradictory results have been obtained. In particular, the fairly large masses of the bulges in the early-type galaxies are difficult to explain by secular evolution alone, related to bar-induced gas infall and subsequent star formation in the central regions of the galaxies (see Kormendy & Kennicutt 2004), at least if no external intergalactic material is added to the bulge. It needs to be re-investigated what is the nature of bulges of S0s in the nearby Universe, e.g. are they disk-like or more likely have properties of merger built structures. Answering this question would set important constraints on models of galaxy formation and evolution.

Scaling relations have been used for theoretical modeling of elliptical galaxies (see de Zeeuw & Franx 1991), and for evaluating the formation of galactic disks in spiral galaxies (Dalcanton, Spergel & Summers 1997; Firmani & Avila-Rees 2000). Therefore, the scaling relations can be used as a tool to study the origin of S0s, which morphologically appear between the two main types of galaxies. One such scaling relation was introduced by Kormendy (1977), who showed, using $R^{1/4}$ models, that the effective radius (r_{eff}) is connected to the central surface brightness (μ_0), both for elliptical galaxies and for bulges of early-type disk galaxies. The dispersion in this so-called Kormendy relation is reduced by adding a third parameter, a Sérsic index n , leading to the photometric plane (e.g. Khosroshahi, Wadadekar & Kembhavi 2000). Alternatively, if the central velocity dispersion is used, the fundamental plane is obtained (e.g. Djorgovski & Davis 1987; Dressler et al. 1987). Other important scaling relations appear between the brightnesses and the scale parameters of the bulge and the disk (Courteau, de Jong & Broeils 1996), and between the brightness of the bulge with the total galaxy brightness (Yoshizawa & Wakamatsu 1975; Carollo et al. 2007).

The scaling relations studied for the S0 galaxies so far are open to different interpretations: while the fundamental plane and the Kormendy relation have associated their bulges with the elliptical galaxies (Pahre, Djorgovski & Carvalho 1998; Pierini et al. 2002; Aguerri et al. 2005a), the scale parameters of the bulge and the disk hint to a spiral origin (Aguerre et al. 2005a; Laurikainen et al. 2009). In a broader context, scaling relations for spiral galaxy samples have been extensively studied revealing several fundamental relations (see Ravikumar et al. 2006; Graham & Worley 2008 as some of the latest works). However, the spiral samples contain just a small number of S0s, which makes it difficult to draw conclusions about S0 properties. In addition, except for the first attempts by Aguerri et al. (2005a) and Laurikainen et al. (2009), the scaling relations for the disk galaxies have not yet been studied using a 2D multi-component approach, which is important in accounting for structure, particularly in barred disk galaxies (Peng 2002; Laurikainen et al. 2004, 2006; Gadotti 2008).

In this study the photometric scaling relations are studied for a sample of 175 early-type disk galaxies, mainly S0s in NIRS0S. This is the largest sample of S0s studied in detail up to now. We use deep K_s -band images for decomposing the two-dimensional surface brightness image to structure components, including bars, ovals and lenses. We present new decompositions for 122 galaxies, and use our previously published decompositions for the rest of the NIRS0S sample. As a comparison sample we use the Ohio State University Bright Spiral Galaxy survey (OSUBSGS; Eskridge et al. 2002) of nearly 200 spirals, for which similar multi-component decompositions have been previously made by us (Laurikainen et al. 2004). Our main emphasis is to compare whether the photometric properties of bulges in S0s are more similar to those of elliptical galaxies or bulges in spirals. Also, implications of these scaling relations for the formative processes of bulges in S0s are discussed. Our uniform decomposition approach, applied for a statistically significant sample of galaxies, using deep K_s -band images, allows us to re-evaluate the properties of bulges and disks in S0s, and to make an unbiased comparison with spirals.

2 SAMPLE AND OBSERVATIONS

Our primary sample consists of 175 early-type disk galaxies, mainly S0s (117 S0s, 22 S0/a-Sa, 36 Sa galaxies). It is part of the Near-IR S0 galaxy Survey (NIRS0S) of 184 galaxies, with the following selection criteria from the Third Reference Catalog of Bright Spiral Galaxies (de Vaucouleurs et al. 1991; hereafter RC3): $B_T \leq 12.5$ mag, inclination $\leq 65^\circ$, and Hubble type $-3 \leq T \leq 1$ ¹. Some of the observed galaxies lie outside the original sample limits for various reasons, usually due to specific weather conditions, e.g. high wind speed, that prevented us from accessing the original sample galaxies. In such circumstances we often observed a somewhat fainter galaxy ($B_T < 12.8$) than in our original sample. In order not to miss the S0s that might be erroneously classified as E galaxies in the RC3, our sample includes also E galaxies classified as S0s in the Revised Shapley Ames Catalog of Bright Galaxies (Sandage & Tammann 1981, hereafter RSA). We emphasize that in the current study it is not in our interest to re-classify galaxies in the near-IR, instead optical classifications are used. The observations and the data reductions are described by Salo et al. (2009, in preparation; hereafter SLBK). The non-rebinned 2D images typically reach the surface brightness level of 21-22 mag arcsec⁻² in the K_s -band. The flux calibrations use multiaperture flux measurements in the K -band, obtained from the Two Micron All-Sky Survey (2MASS)² (Skrutskie et al. 2006). The orientation parameters are from SLBK, where deep V -band images were used when available, otherwise K_s -band images were used.

As a comparison sample we use the Ohio State University Bright Spiral Galaxy Sample (OSUBSGS; Eskridge et al. 2002), which consists of nearly 200 spiral galaxies, covering the Hubble types S0/a-Sm. The selection criteria in OSUBSGS are similar as in NIRS0S except that the apparent magnitude limit is $B_T=12.0$ mag. For 180 of these galaxies we have previously made multi-component decompositions in the H -band using the same method as applied in this study for NIRS0S galaxies (see Laurikainen et al. 2004). In order to convert the parameters of the bulge and the disk of these decompositions to magnitude units, the images were flux-calibrated using the total K -band magnitudes given in 2MASS. We thus implicitly assume that the $H - K$ color is constant throughout the galaxy. As a consistency check we compared and found a good agreement of the photometric parameters for those Sa spirals which are common in the NIRS0S and OSUBSGS samples. It is worth noticing that NIRS0S covers the Sa type bin better than OSUBSGS which is why in this study OSUBSGS is used for the Sab-Sm galaxies only.

3 2D MULTI-COMPONENT DECOMPOSITIONS

3.1 Algorithm

We use a 2D multi-component code, BDBAR (Laurikainen et al. 2004; Laurikainen, Salo & Buta 2005), for decomposing the 2D light distribution of galaxies into bulges, disks, bars, ovals and lenses. This approach has turned out to be important, not only for barred galaxies (Peng 2002; Laurikainen et al. 2004), but also for galaxies with ovals and lenses (Prieto et al. 2001; Laurikainen et al. 2005, 2009), since these components can have a significant contribution to the total light. Bars in the decompositions have been modeled also by Prieto et al. (1997), Aguerri et al. (2005a), Reese et al. (2007), Gadotti (2008) and Weinzirl et al. (2009). Quantitatively the effect of bars on the fitted model was studied by Laurikainen et al. (2006), who compared 2D bulge/disk decompositions with bulge/disk/bar decompositions for a sample of 15 S0-S0/a galaxies. They showed that the mean bulge-to-total (B/T) flux-ratio changed from 0.55 to 0.30 and the mean Sérsic index n from 2.6 to 2.1 when bars were taken into account. Including also nuclear bars reduced the mean B/T flux ratio even further to 0.25. Obviously, bulge/disk decomposition and multi-component approaches represent different views of the concept of the bulge: in simple bulge-disk decompositions for strongly barred and lens-dominated galaxies the B/T flux ratio is more like a concentration parameter than a measure of the relative amount of light in the spheroidal component. In the multi-component approach, B/T allows us to measure the relative amount of light of the bulge in a more reliable manner. This is expected to have implications for the parameters of the bulge and disk, which has to be taken into account when comparing our results with those obtained previously in the literature. As many S0 galaxies have weak outer disks, it is sometimes useful to apply the 1D decomposition approach (Laurikainen & Salo 2000) first, which, due to the azimuthal averaging, gives the scale length of the disk in a more robust manner.

In our 2D decomposition code all components use generalized elliptical isophotes, the isophotal radius being described as:

$$r = (|x|^{c+2} + |y/q|^{c+2})^{1/(c+2)}.$$

¹ Our current NIRS0S sample differs from that specified by Laurikainen, Salo & Buta (2005) and Buta et al. (2006) in that we use B_T or the photographic value m_B , or the average of these two when both are available. This was done to eliminate contamination of the original sample by total V magnitudes in RC3, which occupy the same column as B_T in that catalog.

² The Two Micron All Sky Survey, which is a joint project of the University of Massachusetts and the Infrared Processing and Analysis Center/California Institute of Technology, is funded by the National Aeronautics and Space Administration and the National Science Foundation

The isophote is boxy when the shape parameter $c > 0$, disk when $c < 0$, and purely elliptical when $c = 0$. Circular isophotes correspond to $c = 0$ and minor-to-major axial ratio $q = 1$. Here the x-axis is along the apparent major axis of the component, having a position angle ϕ at the sky. The origin is at the galaxy center, taken to be the same for all components.

The disk is described by an exponential function:

$$I_d(r_d) = I_o \exp[-(r_d/h_r)],$$

where I_o is the central surface density, and h_r is the scale length of the disk. The radius r_d is calculated along the disk plane defined by the assumed position angle ϕ_d and axial ratio q_d of the disk. I_o is in flux units, and when converted to magnitudes it is denoted by μ_o .

The surface brightness profile of the bulge is described by a Sérsic's function (Sérsic 1963, 1968):

$$I_b(r_b) = I_{ob} \exp[-(r_b/h_b)^\beta],$$

where I_{ob} is the central surface density, h_b is the scale parameter of the bulge, and $\beta = 1/n$ determines the slope of the projected surface brightness distribution of the bulge ($n = 1$ for an exponential, and $n = 4$ for the $R^{1/4}$ -law). I_{ob} expressed in magnitudes is denoted by μ_{ob} . The parameter r_b is the isophotal radius defined via the parameters q_b , c_b and ϕ_b , where the subscript stands for bulge. The effective radius of the bulge, r_{eff} , is the half light radius of the bulge (the radius of the isophote that encompasses half of the total bulge light), obtained by numerically integrating over the profile. According to Möllenhoff & Heidt (2001) for $\beta > 0.2$ a good approximation is provided by:

$$r_{eff} = (2/\beta - 0.33)^{1/\beta} h_b.$$

The Sérsic function can be applied for any non-axisymmetric component, or alternatively the Ferrers function can be used (Section 3.2 specifies when these functions are used), described as:

$$I_{bar}(r_{bar}) = I_{obar} (1 - (r_{bar}/a_{bar})^2)^{n_{bar} + 0.5}, \quad r_{bar} < a_{bar}$$

$$I_{bar}(r_{bar}) = 0, \quad r_{bar} > a_{bar},$$

where I_{obar} is the central surface brightness of the bar component, a_{bar} is the component major axis length, and n_{bar} is the exponent of the model defining the shape of the radial profile. The isophotal radius, r_{bar} , is defined via the parameters q_{bar} , c_{bar} and ϕ_{bar} . In the equation the designations are for a bar, but they can refer to any non-axisymmetric component.

3.2 Fitting procedure

The decompositions will be used for two purposes: (1) for morphological analysis, and (2) for adjusting the images to face-on orientation. For the morphological analysis we use the full advantages of the algorithm, whereas for adjusting the images we need to assume that the bulges are spherical. This is because it is not possible to convert a non-circular 2D brightness distribution into 3D space density in a unique manner. The inclination-corrected images will be used in a forthcoming paper while analyzing the properties of bars.

Fitting is done in flux units using a weighting function where the pixel weights are inversely proportional to Poisson noise. However, as shown by Laurikainen, Salo & Buta (2005) the weighting function is not critical for the obtained model. In order to account for the effects of seeing, the fitted model is convolved with a Gaussian PSF, based on the stellar FWHM measured for each image. To obtain reasonable solutions the main structural components need to be identified first. The identifications were made based on isophotal analysis (see SLBK), and on inspection of the original images: the distinction between bars and ovals is based on the ellipticity of the structure (ovals have lower ellipticities), whereas the division between ovals and lenses is not always clear (see Section 5.2 for a definition of bars, ovals and lenses). Bars are generally fitted by a Ferrers function using $n_{bar} = 2$, whereas for ovals and lenses $n_{bar} = 1$ or 0 are used, giving flatter light distributions and sharper outer edges. The small n_{bar} -values for the lenses are justified because the lenses presumably have a small vertical thickness and the flux drops fairly quickly at the outer edge. Ovals are assumed to have a larger vertical thickness, but the division between ovals and lenses is not always clear. The Sérsic function generally worked well for the inner disks, but in a few cases it has also been used for a bar.

The fitting strategy is the same as used by Laurikainen et al. (2004, 2005, 2006). Preliminary solutions were obtained using the images re-binned by a factor of 4, but the final solutions were found using the full image resolution. In simple cases where the galaxies have only a bulge, an exponential disk and a bar, the solutions were generally found automatically. However, in more complicated cases (a large majority of the galaxies) an iterative approach was used. The scale length of the disk, h_r , was found first; if the disk was faint the 1D code was used to find h_r . The other components were found one by one, fixing some of the parameters and leaving the critical parameters free for fitting. The parameter n_{bar} in the Ferrers function

was not left free for fitting, otherwise the models for bars, ovals and flattened bulges become easily degenerate. Galaxies that have a secondary bar typically also have a bright oval surrounding it. As the oval can be as bright as the bar, in some cases both components were fitted by a single Ferrers function. Once a satisfactory solution was found, based on inspection of the model image and the fit to the surface brightness profile, all parameters were left free for fitting. However, this last step was not always possible. Finally, we checked whether the whole surface brightness profile can be fitted by a single Sérsic function: this was done to guarantee that we are not erroneously classifying an elliptical galaxy as an S0. The seeing FWHM gives a theoretical lower limit for the smallest components in the model. However, the central components fitted in this study are nuclear bars or disks which clearly exceed this size limit. The outer disk is fitted to a maximum radial distance where the galaxy is still visible, limited by the standard deviation of the sky background.

3.3 Individual cases

The decompositions are shown in Figure 1. For each galaxy the right panel shows the decomposition, whereas in the two left panels the original image (upper panel) and the model image (lower panel) are shown. The profiles are shown both in linear and in logarithmic radial scales. The y-axis in the right panel is the surface brightness given in mag arcsec⁻² and the x-axis is the radius along the sky plane given in arcseconds, and plotted are the pixel values. In such a presentation a spherically symmetric component appears as a curve, while non-axisymmetric components fill an area confined by their major and minor axis exponential profiles. Exponential disk component fills a wedge-shaped region when a linear radial scale is used. A few representative examples are shown in the paper version, whereas the decompositions for the rest of the galaxies are available in electronic form.

ESO 208-G21 is an example of a sample galaxy which turned out to be an elliptical galaxy, in agreement with its classification in the RC3, while ESO 137-G10 is well represented by a simple bulge/disk decomposition. For ESO 208-G21 the surface brightness profile declines smoothly, whereas ESO 137-G10 has a transition zone between the bulge and the disk. ESO 208-G21 also has a small inner disk. IC 5328 and NGC 524 are two examples of non-barred galaxies with prominent lenses: IC 5328 has one prominent lens, whereas NGC 524 has at least two lenses, both identified as exponential sub-sections in the surface brightness profile, indicating that multi-component decomposition is preferred. In both cases the lenses are significant enough to affect the parameters of the bulge. Examples of barred galaxies are NGC 6782 and NGC 2950: for NGC 6782 two Ferrers functions are used, one for the nuclear bar and the lens surrounding it, and another for the primary bar and a lens, ending at an inner ring (B+L). NGC 2950 has two bars and a lens extending outside the primary bar (B,B,L). Some of the S0s and S0/a galaxies in our sample have bulges that are exceptionally small for their Hubble type (NGC 6654 and NGC 4696): such small bulges can appear both in barred (NGC 6654) and in non-barred (NGC 4696) galaxies. NGC 4696 is classified as an elliptical galaxy in the RC3, but the galaxy clearly has an exponential disk and a prominent lens. In NGC 6654 the secondary bar is important for making a good fit to the intermediate zone between the bulge and the primary bar. The main parameters of the bulge and the disk, as well as the inclination used, are collected in Table 1. The decompositions for the individual galaxies are discussed in Appendix A.

4 CALCULATION OF THE STRUCTURAL PARAMETERS

The correlations we wish to investigate need to be based on parameters corrected for Galactic and internal extinction, as well as for inclination. For this purpose, we use the following corrections derived by Graham & Worley (2008, hereafter GW2008) and Driver et al. (2008):

$$h_r^o = h_r / C_1$$

$$\mu_o = \mu_0^{obs} - A_g(K) - C_2$$

$$M_K^o(bulge) = K(bulge) - A_g(K) - C_3 - 5 \log D - 25.0$$

$$M_K^o(disk) = K(disk) - A_g(K) - C_4 - 5 \log D - 25.0$$

$$C_1 = 1.02 - 0.13 \log(\cos i)$$

$$C_2 = 0.06 + 0.79 (2.5 \log(\cos i))$$

$$C_3 = 0.11 + 0.79 (1 - \cos i)^{2.77}$$

$$C_4 = 0.04 + 0.46 (1 - \cos i)^{4.23}.$$

In these equations D is the galaxy distance in Mpc, taken either from the Catalog of Nearby Galaxies (Tully 1988) or from NED, based on $H_o=75 \text{ km s}^{-1} \text{ Mpc}^{-1}$. $M_K^o(\text{bulge})$ and $M_K^o(\text{disk})$ are the absolute magnitudes of the bulge and the disk, and μ_o is the central surface brightness of the disk, all corrected for Galactic and internal extinction. In addition, μ_o has also been corrected to face-on orientation. The Galactic extinction, $A_g(K)$, is taken from NED and is based on the maps of Schlegel, Finkbeiner & Davis (1998). The parameters C_1 - C_4 are the corrections for internal dust and depend on the inclination i of the disk. C_1 and C_2 are based on constants appropriate to the K -band taken from Table 1 of GW2008, while the constants C_3 and C_4 are from Driver et al. (2008). Following GW2008, we do not apply any intrinsic dust corrections for the Sérsic parameters of the bulge (n, r_{eff}) because these corrections are not well known. However, as we are working in the infrared, the effects of dust are not expected to be severe. Also, we don't apply any cosmological dimming correction because the galaxies studied are fairly nearby systems. The magnitude of the bulge is based on the flux of the bulge model, whereas the magnitude of the disk uses the flux obtained by subtracting the bulge flux from the total model (e.g., it includes possible bar/oval/lens components). The fluxes are calculated inside the maximum radial distance used in the decomposition (not extrapolated to infinity). The dust corrections in the above equations by GW2008 and Driver et al. (2008) are based on 3D radiative transfer models, using the recent determination of the opacity in face-on nearby disk galaxies, based on the Millennium Galaxy Catalogue of nearly 10000 galaxies.

5 ANALYSIS OF THE STRUCTURE PARAMETERS

For the NIRS0S sample the parameters of the bulge and the disk are compared mainly in three groups of galaxies: (1) S0 vs S0/a-Sa galaxies, (2) barred vs non-barred S0s, and (3) galaxies with high vs low luminosity bulges, using the median value $M_K^o(\text{bulge}) = -22.7 \text{ mag}$ as a dividing line. In K -band the S0s in our sample are on average 0.3 mag brighter than the S0/a-Sa galaxies, with mean absolute brightnesses, M_{tot} , -24.0 ± 0.1 and $-23.7 \pm 0.1 \text{ mag}$, respectively. The uncertainties denote the standard errors of the mean. However, taking into account the morphological bin-to-bin variations among S0s in NIRS0S, this difference is insignificant. In the following, the OSUBSGS sample is generally divided in two morphological type bins: Sab-Sbc, and Sc and later. This is because the galaxy brightness is maintained nearly constant for S0-Sbc, after which it drops by almost one magnitude. Compared to optical surface photometry, the use of near-IR images yields parameters that are less biased by differences in age and metallicity of the stellar populations (de Jong 1996), and are also less affected by dust (Cardelli, Clayton & Mathis 1989).

5.1 Galaxies included in the statistical analysis

Based on the presence of the disk, 15 NIRS0S galaxies were included as S0s, even though they are listed as elliptical galaxies in RC3. These galaxies are: IC 4889, IC 5328, NGC 584, NGC 1344, NGC 2768, NGC 4696, NGC 4976, NGC 5419, NGC 5846, NGC 5898, NGC 6482, NGC 6958, NGC 7029, NGC 7192 and NGC 7796. In most cases these galaxies are classified as S0s also in the Revised Shapley Ames Catalog of Bright Galaxies (Sandage & Tammann 1981) and in the Carnegie Atlas of Galaxies (Sandage & Bedke 1994, hereafter CAG). The fact that many, particularly late-type ellipticals are mis-classified S0s is consistent with the recent result by van den Bergh (2009). In our original sample truly elliptical galaxies (best fit by a single $R^{1/n}$ profile) appeared to be NGC 439, NGC 3706, NGC 5982 and ESO 208-G21. Of these NGC 5982 is classified as elliptical galaxy in the RC3, whereas the other 3 galaxies are classified as S0s.

From the subsequent statistical analysis the following galaxies are eliminated: (1) the elliptical galaxies indicated above, and (2) dwarf galaxies (having absolute magnitudes less than $M_B = -18 \text{ mag}$, see Sandage & Binggeli 1984), including NGC 4531 and NGC 5206. We also excluded NGC 3900, for which the decomposition was considered uncertain. For NGC 4369 and NGC 4424, the parameters of the bulge were not reliable, mainly because the number of pixels used in the bulge model was too small and these two were eliminated from the bulge statistics. There are also decompositions in which the bulge model was considered fairly reliable in spite of the fact that the disk could not be fitted in a reliable manner. These galaxies are: NGC 1415, NGC 3166, NGC 3998, NGC 4369, NGC 4457, NGC 4772, NGC 5631, NGC 7029 and NGC 4612. They were eliminated from the statistics when discussing the disk parameters, but included in the analysis of the bulges. For the analysis of the bulges we ended up with 151 galaxies, and for the analysis of the disks with 142 galaxies.

5.2 Identification of the structural components: bars, ovals and lenses

Identification of the structural components was made before starting the decompositions, which was to ensure that only physical structures were fitted. The only exceptions are the faint structures that appear only in the residual images after subtracting the bulge or disk model functions. If not otherwise mentioned, we include as barred galaxies all those systems in

which the bar is visually identified in the image, or is visible in the residual image after subtracting the bulge model from the original image. Bars identified by eye generally appear as bars also in the isophotal and Fourier analysis: they appear as a bump in the ellipticity profile, the position angle being maintained nearly constant in the bar region (see SLBK). In the bar region there is also a peak in the radial A_2 amplitude profile, where A_2 is the $m = 2$ Fourier density amplitude normalized to $m = 0$ (see for example Buta et al. 2006). There are 10 galaxies in the sample in which the bar is visible only after subtracting the bulge model from the original image: NGC 484, NGC 507, NGC 1161, NGC 1351, NGC 2768, NGC 2902, NGC 3998, NGC 4373, NGC 7377 and IC 5328. For NGC 3998 the profile was shown in Laurikainen et al. (2009). For 6 of these galaxies there is weak evidence for a bar also in the A_2 and in the ellipticity profiles, whereas in the other galaxies the bar is completely overshadowed by the bulge flux. Whenever a galaxy has a clear bar based on the A_2 and the ellipticity profiles, the galaxy also appeared barred when inspecting the image visually.

Ovals are global deviations from the axisymmetric shape in galactic disks (see Kormendy & Kennicutt 2004). In the isophotal and Fourier analysis they generally appear qualitatively in a similar manner as bars. However, in contrast to bars, they have lower ellipticities, $b/a > 0.85$ (Kormendy & Kennicutt 2004), and therefore lack significant Fourier terms higher than $m = 2$ (Laurikainen et al. 2007).

Lenses are defined as components with a shallow or constant surface brightness profile, and a sharp outer edge (see Kormendy & Kennicutt 2004). As lenses can also appear as axisymmetric structures they cannot be identified in a similar manner as bars and ovals. In addition, if the bulges are very prominent the lenses may not be directly visible in the images, but can be identified in the residual images after subtracting the bulge model. The early papers by Burstein (1979), Tsikoudi (1980) and Kormendy (1979, 1982) discussed that the lenses in some face-on S0 galaxies can appear as nearly exponential subsections in the surface brightness profiles. Later, Sandage & Bedke (1994) used this characteristic, “three-zone structure” as part of the classification of S0 galaxies. Recently the exponential sub-sections in the surface brightness profiles have been used to identify lenses in S0s in a systematic manner (Laurikainen et al. 2005, 2006, 2009). However, it is worth noticing that the exponential sub-sections in the surface brightness profiles are not always interpreted as lenses: Erwin, Beckman & Pohlen (2005) suggested that they can be manifestations of anti-truncated disks inside more spheroidal-like components such as bulges or halos.

In this study, we use the exponential sub-sections in the surface brightness profiles as suggestions for lenses. This is justified, because in most cases the exponential sub-sections can be directly associated with lenses in the images. In barred galaxies, the lenses often have a specific orientation with respect to the bar. In many S0s multiple lenses appear, extending to the largest visible radial distance in the image, which rules out the possibility that they were truncated disks inside more extended spheroidals. In any case, for the present goal of deriving the scaling relations of S0s, the detailed interpretation of lenses is not crucial, as long as they are accounted in the decompositions so that their presence does not affect the derived parameters of the bulge.

6 PARAMETERS OF THE BULGE AND THE DISK

6.1 Kormendy relation

It has been suggested by Kormendy (1977) that both elliptical galaxies and bulges of S0s show a strong correlation between the central surface brightness (μ_{ob}) and the effective radius (r_{eff}), subsequently known as the Kormendy relation. It was shown later that the surface brightness at the effective radius of the bulge (μ_{eff}) is actually a better estimate of the surface brightness because it is not as much affected by seeing and is also less model dependent (Djorgovski & Davis 1987). Using the mean surface brightness inside r_{eff} (denoted by $\langle \mu \rangle_{eff}$) further minimizes the effects of the measurement uncertainties. In the early studies the $R^{1/4}$ function was used, but later studies have shown that the Sérsic function, $R^{1/n}$, gives a better fit for the elliptical galaxies (Caon, Capaccioli & D’Onofrio 1993), and for the bulges of S0s (Andredakis, Peletier & Balcells 1995; Balcells et al. 2003). Differences are expected in the photometric parameters obtained using the $R^{1/4}$ and the $R^{1/n}$ functions, particularly if the images are not very deep (Trujillo et al. 2002), but these variations are not expected to affect the Kormendy relation (Ravikumar et al. 2006).

The Kormendy relations for the NIRS0S and OSUBSGS galaxies are shown in Figure 2. In this and in all the following figures the S0 class consists of the Hubble types $S0^-$, $S0^0$ and $S0^+$. For comparison, the line for the bright Coma cluster ellipticals is also shown, taken from Khosroshahi et al. (2000). In Figure 2, $\langle \mu \rangle_{eff}$ is used (rather than μ_{eff}) and it is calculated from the flux calibrated images in a similar manner as in Khosroshahi et al. (2000) (taking into account the difference in the Hubble constant H_0 used in the two studies). It appears that although S0s are located close to the elliptical galaxies, as a group they are offset by 0.3 mag (at a median r_{eff} of 0.58 kpc) from the bright Coma cluster ellipticals. For S0/a-Sa galaxies the offset is 0.7 mag (at a median r_{eff} of 0.51 kpc). It is also worth noticing that the brightest bulges (those

brighter than $M_K^0(\text{bulge}) = -22.7$ mag), both among the S0s and S0/a-Sa galaxies, behave in a similar manner as the elliptical galaxies in the Kormendy relation (a similar result is obtained if the S0 sample is divided in two bins, based on the total absolute galaxy brightness, using $M_{tot} = -24.5$ mag as a dividing line). Our sample includes also S0s with r_{eff} smaller than obtained for any of the Coma cluster ellipticals. In spite of their small size, they do not fall in the region of the dwarf elliptical galaxies (dE) with a similar r_{eff} (see Capaccioli & Caon 1991; Khosroshahi et al. 2004; Ravikumar et al. 2006): for a given r_{eff} , the dE's have several magnitudes lower surface brightnesses than the bulges of our sample galaxies. The offset we had between S0s and ellipticals differs from previous studies obtained in the optical (Kormendy 1984; Capaccioli, Caon & D'Onofrio 1992) and in the near-IR (Pahre, Djorgovski & Carvalho 1998; Pierini et al. 2002; Ravikumar et al. 2006), according to which the Kormendy relations are similar for the S0s and for the bright elliptical galaxies: hence we find that they are, in fact, offset.

For spirals, the Kormendy relation has previously been studied by many groups. In an early study by Kormendy (1984), the bulges were found to follow the same relation as the elliptical galaxies, but later studies showed that spiral galaxies actually lie below the bright elliptical galaxies, and also have a larger dispersion (Kent 1985; Kodaira, Watanabe & Okamura 1986; Khosroshahi et al. 2000; Capaccioli, Caon & D'Onofrio 1992; Hunt, Pierini & Giovanardi 2004; Ravikumar et al. 2006; GW2008). The dispersion is largest for the late type spirals (Ravikumar et al. 2006). Our study for OSUBSGS and NIRS0S spirals confirms the above tendencies: the S0/a-Sa galaxies appear slightly below the bright ellipticals (and S0s), whereas the later types are more dispersed towards lower surface brightnesses. Ravikumar et al. (2006) have shown that faint spirals with $M_K > -22$ mag do not obey the same Kormendy relation as the brighter galaxies (see also Capaccioli & Caon 1991). Using a limiting absolute magnitude of -22.7 mag for the bulges, we see a similar effect.

6.2 Photometric plane

The photometric plane for early-type galaxies was first addressed by Scodreggio, Giovanelli & Haynes (1997), who added a third parameter to the Kormendy relation, namely the difference between the galaxy magnitude and the characteristic magnitude of the cluster. Compared to the fundamental plane using velocity dispersion as the third parameter, it has the advantage of making the relation achievable with photometry alone. Compared to the Kormendy relation the dispersion is smaller, but it can be used only for galaxies in clusters. The photometric plane for more general use was addressed by Khosroshahi, Wadadekar & Kembhavi (2000): it was defined by μ_{ob} , r_{eff} and the Sérsic index n which, compared to the Kormendy relation, likewise reduces the dispersion. The photometric plane for bright elliptical galaxies has been studied also by Graham (2002), who replaced μ_{ob} with μ_{eff} .

In this study, we use the photometric plane as defined by Khosroshahi Wadadekar & Kembhavi (2000). In order to study the photometric plane Khosroshahi et al. (2000) used K -band images of a sample of 26 non-barred S0-Sbc galaxies. They found that the bulges of these galaxies which are mainly spirals (including 6 S0s), occupy the same region in the photometric plane as the bright Coma cluster ellipticals. On the other hand, Méndez-Abreu et al. (2008) found that bulges of S0s appear in the same region as the bulges of early-type spirals, though they did not investigate whether these galaxies are located also in the same region as the elliptical galaxies. Their sample consisted of 148 non-barred S0-Sb galaxies (mainly S0s, including 58 spirals) and they used J -band images taken from 2MASS.

The photometric plane for the NIRS0S and OSUBSGS galaxies is shown in Figure 3, again comparing it with the bright Coma cluster ellipticals. We can see that in the photometric plane bulges of S0s typically lie slightly below the elliptical galaxies, indicating that, for a given r_{eff} or μ_{ob} , they have a smaller Sérsic index than the elliptical galaxies. When extrapolating the line for the bright ellipticals to lower r_{eff} , the deviations of S0s from the elliptical galaxies increase. Compared to spirals, the S0s form a more homogeneous group of galaxies: spiral galaxies have a larger dispersion which increases towards lower r_{eff} and later Hubble types. In the photometric plane the barred and non-barred S0s occupy the same region.

Our result for early-type spirals (S0/a-Sa galaxies are not like the ellipticals) thus deviates from that of Khosroshahi et al. (2000), and slightly also from that of Méndez-Abreu et al. (2008) (the early-type spirals do not behave exactly like the S0s). A possible reason for these differences is likely to be our use of deeper images and the use of multi-component decompositions. It is also worth noticing that the brighter galaxies in the NIRS0S sample deviate from the elliptical galaxies more than the fainter galaxies. The spiral galaxies Sab-Sbc are located below the Coma cluster elliptical, in a similar manner as the S0/a-Sa spirals.

6.3 Bulge-to-total flux ratios

The distributions of bulge-to-total (B/T) flux ratios for the galaxies in the NIRS0S and OSUBSGS samples are shown in Figure 4. Bulge-to-disk (B/D) flux ratios for the OSUBSGS galaxies were taken from Laurikainen et al. (2004) and converted to B/T flux ratios. The B/T -values in both samples were corrected for the effects of Galactic and internal dust using the equations in Section 4, applying different corrections for the bulge and the disk. The corrected mean B/T values in different

Hubble type bins are shown in Table 2. The values we find for S0-S0/a galaxies are consistent with $B/T \sim 0.25$ - 0.28 as found previously by Balcells et al. (2003, 2007) for non-barred galaxies, and by Laurikainen et al. (2005, 2006), Gadotti (2008), and Weinzirl et al. (2009) using a multi-component approach. For later type galaxies in the OSUBSGS sample, similar low B/T values have been obtained also by Weinzirl et al. (2009).

Fig. 4. shows the characteristic peaks in the B/T distribution for the different Hubble type bins. The rather wide spread for each bin reflects the fact that the bulge was not the only criterion in the original Hubble classification of galaxies. In the original classification the bulges played a more important role for the early-type galaxies than for the later types, where the spiral arms were the dominating feature. Using deep K_s -band images, applying a multi-component decomposition method, and including proper dust corrections, we are in a position to re-evaluate the B/T distribution. It appears that the S0 galaxies have a large range of B/T extending to very small values. In particular, the number of S0s with small $B/T \sim 0.10$ is 3% ($N=3$), and 13% ($N=12$) have $B/T < 0.15$. If S0/a galaxies are also included the values are 13% and 25%, respectively. Small B/T values, comparable to those obtained for Sc galaxies, have been found previously by Erwin et al. (2003) for two S0s, using both photometric and kinematic data, and by Laurikainen et al. (2006) for one S0, based on a morphological analysis. In our sample, the barred and non-barred S0s have similar B/T flux ratios ($\langle B/T \rangle = 0.29 \pm 0.02$ vs 0.33 ± 0.03 , respectively), which is not fully consistent with Aguerri et al. (2005) and Laurikainen et al. (2007), who found indications that B/T is smaller for barred galaxies. Most probably the difference between barred and non-barred S0s is real, but is so weak that it is visible, at a statistically significant level, only when strongly barred S0s are studied.

In Fig. 5 the B/T flux ratio, Sérsic index n , the bulge effective radius scaled to the disk scale length r_{eff}/h_r^0 , and the total absolute magnitude M_{tot} , are shown as a function of Hubble type (r_{eff}/h_r^0 is discussed in Section 6.6). M_{tot} is the total observed K -band absolute magnitude corrected for Galactic extinction. For the OSUBSGS galaxies B/T and n as a function of Hubble type, have previously been shown by Laurikainen et al. (2007), with the difference that their B/T values were not corrected for internal dust. The B/T values for the OSUBSGS sample has been discussed also by Weinzirl et al. (2009). The symbols denote the median values in each Hubble type bin, and the error bars indicate the standard deviations of the mean. For comparison, the median values from GW2008 are also shown. They compiled all reliable decompositions from the literature, leading to a sample of 400 disk galaxies, including 16 S0s. In Fig. 5, the mean B/T and n are almost constant for S0⁻, S0^o, S0⁺, S0/a and Sa galaxies, except that B/T increases gradually towards S0⁻ types. A small drop in the B/T flux ratio towards the early-type S0s found by Laurikainen et al. (2007) is not seen here (their sample consisted of a sub-sample of only 37 S0s of NIRS0S representing mainly barred galaxies). Note that a small B/T (and n) value for S0s is given also by GW2008, however this is based on 16 galaxies from the NIRS0S sample, belonging to the above-mentioned sub-sample.

For spiral galaxies in the OSUBSGS sample the mean B/T flux ratio decreases from Sab towards later types, in agreement with GW2008, shown also in many previous studies (see the references in GW2008). In our study the mean Sérsic index n is only slightly larger for the S0-Sa galaxies than for the later types. It appears that our values for n and to some extent also for B/T , are systematically lower than the values compiled by GW2008. The comparison is meaningful only between S0/a-Sc types, because the number of galaxies is small among the later type galaxies in the OSUBSGS sample, and among the S0s in GW2008. The systematic shift between GW2008 and the current study is most likely explained by the different decomposition approaches used: although GW2008 collected all reliable measurements from the literature, most of them, particularly for the later type galaxies, are based on bulge/disk decompositions. It is expected that excluding the contribution of the bar flux in the decomposition makes the fitted bulge profile shape less exponential and increases the fitted B/T flux ratio (Laurikainen et al. 2006), and likewise also the estimated effective radius.

6.4 Other parameters of the bulge

The total luminosity of a bulge can be expressed by the parameters of the Sérsic function: $L = k_L I_{eff} r_{eff}^2$, where I_{eff} is the flux at r_{eff} (corresponding to μ_{eff}) and k_L is the structural parameter determined by the shape of the light distribution (i.e., by Sérsic n). This implies that due to the Sérsic function alone correlations are expected for $M_K^0(bulge)$ vs r_{eff} , and for $M_K^0(bulge)$ vs μ_{eff} . If $M_K^0(bulge)$ additionally correlates with $M_K^0(disk)$ (as discussed in Section 6.6), then r_{eff} and μ_{eff} are also expected to correlate with the B/T flux ratio, which is the case for S0s. The correlations are weaker when B/T is used instead of $M_K^0(bulge)$, because the contribution of the disk light to the total light varies.

More fundamental relations are: (1) n vs $M_K^0(bulge)$, (2) n vs B/T , and (3) $M_K^0(bulge)$ vs M_{tot}^0 . For the spiral galaxies in the OSUBSGS sample, the Sérsic index n has a clear correlation with $M_K^0(bulge)$ (see Fig. 6a), which confirms the previous result for spirals (Graham 2001b; Möllenhoff & Heidt 2001; Noordermeer & van der Hulst 2007). However, for the S0 galaxies no such correlation is present, at a statistically significant level. On the other hand, there is a correlation between n and B/T , both for the S0 galaxies and spirals (Fig. 6b), again for spirals confirming the previous results (Andredakis, Peletier & Balcells 1995; Graham 2001b; Trujillo et al. 2002; Balcells, Graham & Peletier 2007).

To illustrate how for S0s n can be correlated with B/T , but not with $M_K^0(bulge)$ itself, $M_K^0(bulge)$ is shown as a function of M_{tot}^0 in two Sérsic index bins, using $n = 2.0$ as a dividing line (Fig. 7). Here M_{tot}^0 is the total K -band absolute magnitude,

corrected for Galactic and internal dust, in a similar manner as was done for B/T in Section 6.3. Different dust corrections were applied for the bulge and the disk, with the fluxes of these components being obtained from the decompositions. The left panel shows the NIRS0S galaxies, whereas the right panel shows the OSUBSGS spirals. The dashed lines indicate three different B/T values of 0.01, 0.1 and 1.0. Evidently, for S0s both luminous and less luminous bulges can have a large range of Sérsic indexes (e.g., no correlation exists between $M_K^o(bulge)$ and n). However, within each M_{tot}^o bin the Sérsic index increases with increasing B/T (a correlation exists between B/T and n). Apparently, the OSUBSGS sample can be divided into two main bins using $M_K^o(bulge) = -20$ mag as a dividing line: the more luminous bulges have much more frequently higher values of the Sérsic index and the B/T ratio than the less luminous bulges. This implies that the correlation between $M_K^o(bulge)$ and n for spirals largely follows by lumping the faint and bright bulges together. It seems that the bulges of S0s are fairly similar to the bulges of spirals having $M_K^o(bulge) < -20$ mag.

Clearly, the bulges of S0 galaxies (in NIRS0S) and spirals (in OSUBSGS) are different from the elliptical galaxies (that bulges of spirals are different from elliptical galaxies was shown also by Graham 2001b; their Fig. 14). This is manifested in the r_{eff} vs $M_K^o(bulge)$ diagram (Fig. 8a) where both appear below the elliptical galaxies (shown as a dashed line, taken from GW2008), shown also by GW2008 (see their Fig. 13). These parameters are correlated, at a statistically significant level, for both S0s and spirals. It is also worth noticing that the bulges of S0s are slightly more compact than the bulges of spirals of a similar bulge luminosity. For spiral galaxies the correlation between r_{eff} and $M_K^o(bulge)$ was found previously also by Balcells, Graham and Peletier (2007) for 19 (non-barred) galaxies, but not by GW2008 for a sample 400 disk galaxies (include 16 S0s). A possible reason why this correlation was found by Balcells, Graham & Peletier (2007) and by us, but not by GW2008, is again the decomposition method used: for non-barred galaxies the method of choice (two-component vs multi-component) is not critical, but it does matter when barred galaxies are included. Figure 8 also shows that for a given bulge brightness, the bulges of S0s have typically higher surface brightnesses than the bulges of spirals.

In conclusion, bulges of S0 galaxies are fairly similar to those spiral bulges brighter than $M_K^o(bulge) \sim -20$ mag.

6.5 Parameters of the disk

For both the NIRS0S and the OSUBSGS samples, the main parameters of the disk correlate with each other: with an increasing scale length of the disk (h_r^o) the disk luminosity ($M_K^o(disk)$) increases, and the central surface brightness (μ_o) becomes fainter (see Figs. 9 a,c), shown previously for S0s by Méndez-Abreu et al. (2008). For spirals, the former correlation has been previously demonstrated by Balcells, Graham & Peletier (2007), and the latter by de Jong (1996), Graham & de Blok (2001) and GW2008. In addition, the scale length for S0s increases with increasing galaxy magnitude (M_{tot}^o), as shown previously for S0s by Aguerri et al. (2005b), Bedregal, Aragón-Salamanca & Merrifield (2006) and Méndez-Abreu et al. (2008). Also, the disks of S0s and spirals do not follow the Freeman law (Freeman 1970), pertaining a constant central surface brightness. Instead, μ_o has a large dispersion (Fig. 9b), as shown previously for spiral galaxies Möllenhoff & Heidth (2001), Aguerri et al. (2005b) and Balcells, Graham, Peletier (2007), and for S0s by Aguerri et al. (2005b) and Méndez-Abreu et al. (2008).

The Figure 9 further demonstrates that the S0 galaxies are located at the same regions with the spiral galaxies, including the late-type spirals. In GW2008 S0s were dispersed to lower μ_o (see their Fig. 8). For S0s in NIRS0S the range in h_r^o is found to be 1-10 kpc, which is very similar to that obtained for spirals, which is larger than that obtained by Aguerri et al. (2005b) and Méndez-Abreu et al. (2008) for S0s (maximum $h_r^o \sim 6$ kpc; see their Fig. 7, based on 2MASS images). Also, $\Delta\mu_o \sim 16-20$ mag for S0s is very similar as the range reported for spirals. To our knowledge the similarity of the disks in S0s and spirals has not been explicitly shown previously, most probably because deep images are needed for detecting the faint outer disks in S0s.

6.6 Parameters of the bulge and the disk cross-correlated

Naively, strong correlations between the parameters of the bulge and the disk are expected if the disks were formed first and the bulges emerged from the disk by secular evolution. Indeed, for spiral galaxies a correlation has previously been found between h_r and r_{eff} (Courteau, de Jong & Broeils 1996; de Jong 1996; Graham & Prieto 1999; Khosroshahi, Wadadekar & Kembhavi 2000; MacArthur, Courteau & Holtzman 2003; Carollo et al. 2007; Noordermeer & van der Hulst 2007). A similar correlation was found also for 15 barred S0 galaxies by Aguerri et al. (2005), and for S0s in the NIRS0S sample by Laurikainen et al. (2009), the latter galaxies following the relation $h_r = 0.62 + 0.46 \log r_{eff}$ (h_r and r_{eff} expressed in kpc). A similar correlation was found by Méndez-Abreu et al. (2008) for a sample of S0-Sb galaxies. For the galaxies in OSUBSGS and NIRS0S samples, this correlation is shown in Figure 10. Clearly, the correlation is similar for all morphological types except that the slope is slightly shallower for the late-type spirals.

Having established the existence of correlations between $M_K^o(bulge)$ and r_{eff} , $M_K^o(disk)$ and h_r^o , and h_r^o and r_{eff} , a correlation between $M_K^o(bulge)$ and $M_K^o(disk)$ is also expected. However, this correlation, shown in Fig. 11, is a direct, and

the most illustrative way to demonstrate how similar or dissimilar the bulges and disks in S0 galaxies and spirals actually are. For spiral galaxies, this correlation has previously been reported by de Jong (1996) and Hunt, Pierini & Giovanardi (2004), and marginally also by Noordermeer & van der Hulst (2007). The exact relation between $M_K^o(bulge)$ and $M_K^o(disk)$ naturally depends on the morphological type, which partly follows from the peaked B/D -distribution in each morphological type bin: a linear correlation means a constant B/D flux ratio, the slope relates to the value of that constant, and the dispersion manifests the variations in B/D for a given morphological type bin. We find fairly similar correlations for S0s and S0/a-Sa galaxies, whereas, as expected, for later types the relative mass of the disk increases. For S0s (in NIRS0S) and Sab-Sbc spirals (in OSUBSGS) we obtain:

$$M_K^o(disk) = 0.63 M_K^o(bulge) - 9.3 \text{ (S0s)}$$

$$M_K^o(disk) = 0.38 M_K^o(bulge) - 15.5 \text{ (Sab-Sbc)}$$

Contrary to what was obtained by Hunt, Pierini & Giovanardi (2004) for spirals, in our study the correlation between $M_K^o(bulge)$ and $M_K^o(disk)$ is equally good for galaxies with small and large Sérsic indexes, where we use $n=2.0$ as a dividing line (not shown in any figure). It is worth noticing that S0s and S0/a-Sa galaxies have very similar bulge and disk luminosities. The relative disk luminosity increases towards late-type galaxies, and decreases towards galaxies with luminous bulges, which is the case for all Hubble types. The range of bulge luminosity is fairly similar for S0-Sbc galaxies, $M_K^o(bulge) \sim -19 - -25$ mag, whereas for Sc-Scd types $M_K^o(bulge) \sim -16 - -22$ mag. This is related to the total galaxy luminosity which drops for the Sc-Scd types.

Due to the correlation $M_K^o(bulge)$ vs $M_K^o(disk)$, a correlation is expected also between $M_K^o(disk)$ and r_{eff} . Indeed, such a correlation is present, both for the S0 galaxies and for spirals in the OSUBSGS sample (Fig. 10a). This correlation was not found by Balcells, Graham & Peletier (2007).

Particularly useful is the parameter r_{eff}/h_r^o , because it can be directly compared to predictions of simulation models, related to galaxy formation and evolution. The median value for r_{eff}/h_r^o for S0s in NIRS0S is 0.20, and for S0/a-Sa galaxies it is 0.15 (Table 2). These values are nearly a factor of two smaller than the value of $\langle r_{eff}/h_r^o \rangle = 0.32-0.36$ obtained for the early-type disk galaxies by Khosroshahi et al. (2000; 26 mainly spirals), Noordermeer & van der Hulst (2007; 19 S0-Sab, mainly spirals), and by Méndez-Abreu et al. (2008; 148 S0-Sb, mainly S0s). For the OSUBSGS spirals we find a median values of $r_{eff}/h_r^o \sim 0.10$, again nearly a factor of two smaller than the median value $r_{eff}/h_r^o \sim 0.22-0.24$ given by GW2008 for spirals, or $\langle r_{eff}/h_r^o \rangle \sim 0.22$ obtained by MacArthur, Courteau & Holzman (2003) for the late-type spirals. This difference is most probably related to the different decomposition methods used: in the previous studies the bulge/disk bar decomposition approach was used, which in barred galaxies is expected to overestimate the flux of the bulge, and therefore also r_{eff} . De Jong (1996) found $\langle r_{eff}/h_r^o \rangle \sim 0.15$ in K -band, but in this early study a constant Sérsic index was used.

7 DISCUSSION

In the current paradigm of galaxy formation, the hierarchical Λ CDM cosmology, simulations have suggested that mergers of primordial disk galaxies form the first elliptical galaxies (e.g., Barnes & Hernquist 1992; Naab, Khochfar & Burkert 2006). The most massive ellipticals or spheroidals are suggested to form in a merger of two gas-poor (dry) ellipticals of a similar mass (e.g., Naab, Burkert & Hernquist 1999; Naab & Burkert 2003), or through multiple or hierarchical mergers (e.g., Weil & Hernquist 1996; Burkert et al. 2008). On the other hand, intermediate mass spheroidals are suggested to form by mergers of an elliptical galaxy with a massive spiral (Khochfar & Burkert 2005; Naab, Khochfar & Burkert 2006). In this picture, a new disk is formed of the gas, which gradually settles into the disk plane from the dark matter halo (Kauffman et al. 1999; Springel & Hernquist 2005). Simulations (Aguerri, Balcells & Peletier 2001; Eliche-Moral et al. 2006; Younger et al. 2007) also show that bulges can form by minor mergers, which are much more frequent in the observed Universe. In these simulations, minor mergers can heat the original disk and trigger a central starburst, which consumes most of the gas in the galaxy, leaving a featureless gas-poor remnant with an outer disk. The bulges formed by minor mergers can be dynamically cooler (Younger et al. 2007; Eliche-Moral et al. 2006), but both in major and minor mergers the formation of bulges and disks is expected to be decoupled.

Cosmological simulations with merger histories (e.g., D’Onghia et al. 2006) have, however, faced serious problems which are not yet fully resolved. For example, they have been unable to unambiguously produce galaxies without classical bulges, or galaxies without any bulges at all. This contradicts the observation that up to 30% of the total stellar mass in nearby disk galaxies might reside in bulge-less galaxies (Kautsch et al. 2006; Cameron et al. 2009). Also, the merger remnants produced in the cosmological simulations are too metal rich, by a factor of 4-8, compared to any observed spheroidals, ellipticals or bulges (Naab & Ostriker 2009). This is the case at least if the mergers appeared at $z > 0.3$.

As an alternative it is possible that the disks were formed first, and the bulges were made of the disk material, followed by subsequent star formation (see Kormendy & Kennicutt 2004 for a comprehensive review). The discovery (Illingworth 1981)

that bulges can rotate and are most likely rotation-flattened oblate spheroids, fits to this picture. This is suggested to be the case for the bulges in low mass spirals (see MacArthur et al. 2008), but might also be an explanation for the bulges of massive disk galaxies, including S0s. Two examples of such low mass bulges in S0s were discussed by Erwin et al. (2003), and more recently, similar cases were found for a sample of early-type galaxies based on integral-field spectroscopy by Cappellari et al. (2007).

7.1 Photometric properties of the bulges in S0s: like ellipticals or more like bulges in spirals?

If the photometric properties of bulges in S0s are similar to those of elliptical galaxies, we may assume that also their formative processes are similar, most probably related to galaxy mergers. On the other hand, if the bulges in S0s resemble more the bulges of spiral galaxies, it is possible that they were formed by secular evolution. However, it is worth noticing that the formation of bulges in all kinds of disk galaxies is under debate, and therefore a possible connection to spirals does not immediately tell what are the physical mechanisms of bulge formation in S0s.

In this study we have discussed many relations between the photometric parameters of the bulge and the disk in S0 galaxies, which link their bulges more tightly to bulges of spirals than to the elliptical galaxies. In fact, bulges of S0s are fundamentally different from the elliptical galaxies, which is manifested in the photometric plane (r_{eff} , μ_{ob} and n ; Fig. 3), in the $M_K^o(bulge)$ vs r_{eff} diagram (Fig. 8a), and to some extent also in the Kormendy relation (r_{eff} and $\langle \mu >_{eff}$; Fig. 2). For S0s, the luminosities of the bulge and the disk correlate with the total absolute galaxy magnitude, and both also correlate with the B/T flux ratio, in a similar manner as found previously for spirals (see Trujillo et al. 2002; Balcells et al. 2003; Carollo et al. 2007).

There is also a group of S0s with $r_{eff} = 0.05$ -0.2 kpc, similar to the values obtained for dwarf elliptical galaxies (dE), but having surface brightnesses several magnitudes higher. Simulations suggest that dwarf galaxies can form from bright galaxies which lose their disks in dense galaxy clusters. However, dwarf galaxies show a large diversity of structures (Lisker et al. 2006), and not all of them are expected to form by galaxy harassment. It is particularly for the disk-like dwarfs (dS0s) that harassment might be at work (Mastropietro et al. 2005). The possibility of several mechanisms being responsible is supported by comparing the photometric properties of dEs and dS0s with the bulges of bright galaxies in clusters (Aguerri et al. 2005b), and also, by comparing the ages and masses of star clusters around pseudobulges in late-type spirals with those obtained in dwarf galaxies (di Nino et al. 2009). However, the simulations by Aguerri & González-García (2009) do not support the view in which also galaxies with initially large bulge-to-disk ratios (presumably early-type disk galaxies) could evolve into early-type dwarfs by galaxy harassment. This simulation result is consistent with our result.

Bulges of S0s have also characteristics that slightly deviate from those obtained for spirals. The faint bulges are slightly more compact than the bulges of spirals of a similar bulge luminosity (Fig. 8a). Also, contrary to spirals, S0s show no correlation between $M_K^o(bulge)$ and the Sérsic index n . (Fig. 6a). These characteristics could manifest environmental effects: the S0s might have had a more prolonged interaction with the intergalactic matter, or with small companions, both of which may have slightly modified their parameters (Scannapieco & Tissera 2003; Naab, Khochfar & Burkert 2006).

We may conclude that the bulges of S0s are photometrically fairly similar to the bulges of spirals, but different from the elliptical galaxies.

7.2 Are the formation of bulges and disks in S0s coupled?

The different formation scenarios of bulges predict different scaling relations for the photometric parameters of the bulge and the disk. The masses and the scale parameters are expected to correlate if the disks were formed first and the bulges emerged from the disk material by secular evolution. On the other hand, in hierarchical clustering the properties of bulges were established already during the merger event (Khochfar & Burkert 2005), and presumably they changed very little after that. The disks continue to grow only slightly in mass and size, due to internal dynamical effects, and due to gas falling into the disk.

In this study, scaling relations are discussed, suggesting that the formative processes of bulges and disks in S0 galaxies are coupled. Most importantly, the absolute brightnesses of the bulge ($M_K^o(bulge)$) and the disk ($M_K^o(disk)$), indicative of their relative masses, are correlated for S0s (a correlation $M_K^o(disk)$ vs r_{eff} follows from this). For S0s in NIRSOS, a correlation exists also between the scale parameters of the bulge (r_{eff}) and the disk (h_r^o) (Laurikainen et al. 2009). Evidently, there must be some regulation process leading to the above correlations.

The scaling relations we obtain for the spiral galaxies in the OSUBSGS sample are similar to those found previously for spirals in many similar studies. An exception is the relation between r_{eff} and $M(disk)$ (Fig. 10) for which Balcells, Graham & Peletier (2007) did not find any correlation. This lack of correlation, together with the lack of correlation between the other parameters of the bulge and the disk ($M_K(disk)$ vs B/T , or $M_K(disk)$ vs $\mu_o(bulge)$) in their study

was considered as a challenge for the secular origin of bulges in spiral galaxies: “bulges do not know how massive their disks are”. However, the sample by Balcells, Graham & Peletier (2007) consisted only of 19 spirals, which might explain the lack of correlation. With our sample of 175 spirals such a correlation is evident, and we conclude that the formation processes of bulges and disks also in spirals galaxies are indeed coupled.

7.3 The formation processes of bulges

The scaling relations discussed above fit a scenario where the disks in a large majority of S0s were formed first, and the bulges emerged from the disk material. In this picture, mass transfer towards the central regions of the galaxies is expected (Athanasoula & Misiroidis 2002), leading to central star formation, thus adding to the mass of the bulge over a timescale of 1-2 Gyrs (Athanasoula Lambert & Dehnen 2005; Bournaud, Combes & Semelin 2005; Debattista et al. 2006; Sarzi et al. 2007). As a consequence, correlations between the masses and the scale parameters of the bulge and the disk appear. However, these scaling relations cannot be unambiguously used to distinguish various formation processes of bulges. A correlation between h_r^o and r_{eff} is expected also if S0s were formed by galaxy mergers: a small companion swallowed by the main galaxy increases the bulge mass, and at the same time the stars in the disk are spread to a larger radius. For spirals we find median $r_{eff}/h_r^o \sim 0.10$, and for S0 galaxies $r_{eff}/h_r^o \sim 0.20$. Compared to the model prediction of $r_{eff}/h_r^o = 0.28-0.33$ by Naab & Trujillo (2006), both values are not well compatible with the merger scenario. Naab & Trujillo constructed simulation models for galaxy mergers using a large range of mass ratios between the main galaxy and the companion. The transport of baryonic matter to the central regions of galaxies by minor mergers increases also the Sérsic index and the mass of the bulge, leading to a correlation between B/T and n (Scannapieco & Tissera 2003; Naab, Khochfar & Burkert 2006). Since secular evolution also produces such a correlation, it does not yield any unique interpretation for the origin of bulges.

In principle, bulges in late-type spirals can be interpreted as disk-like pseudobulges formed by star formation in the disk. Along the same lines, it has been argued that early-type disk galaxies, due to their larger bulge masses, do not have enough gas to produce their bulges in a similar manner. It has been estimated that secular evolution can produce pseudobulges with masses that contain 10% of the total stellar mass in galaxies (Kormendy & Kennicutt 2004). According to Kormendy & Kennicutt this is comparable to $B/T \sim 0.16$. This is still smaller than the new estimates of $B/T = 0.25-30$ for S0s (Laurikainen et al. 2007; Balcells, Graham & Peletier 2007; Gadotti 2008; GW2008; Weinzirl et al. 2009). The estimate by Kormendy & Kennicutt includes only star formation in circum-nuclear rings, so that the B/T -value would be somewhat larger if accretion of external gas (Bournaud & Combes 2002), converted to bulge mass, was also taken into account.

Another way of evaluating the formation processes of bulges is to look at their colors. Bulges formed in a hierarchical clustering scenario are expected to be red, whereas bulges formed recently by disk star formation are naturally blue. However, for example accretion of external gas or small blue companions (Aguerri, Balcells & Peletier 2001) can rejuvenate the bulges. The close relationship between the colours of bulges and disks in spiral galaxies (Peletier & Balcells 1996; MacArthur et al. 2004; Cameron et al. 2009) is consistent with the idea that bulges in spirals were formed by secular evolution. But it has also been suggested by Driver et al. (2006) that the global properties of bulge-disk systems might result from the mixing of a red bulge stellar population with a blue disk population, in varying degrees. Therefore, based on colors it is not yet completely clear whether the bulges in spiral galaxies are intrinsically older, rejuvenated by recent star formation, or if they really are young bulges, produced by secular processes.

7.4 Are S0s descendants of spirals?

The problem related to the fairly large bulge masses in S0s would vanish if we assume that their bulges were formed by galaxy mergers in the distant past. However, in that case the obtained scaling relations for S0s, indicating that the bulges of S0s are not like the elliptical galaxies, or that the formative processes of bulges and disks in these galaxies most probably are coupled, would not have any unambiguous explanation. On the other hand, there are many factors that affect the masses of bulges: a) minor mergers can add mass to an existing bulge, b) dust can obscure massive bulges, particularly in late-type spirals, and c) the most massive bulges in S0s might have been formed at higher redshifts in an environment which is different from that observed in the nearby Universe. Also, not all bulges in S0s are massive: even 13% of them have B/T ratios as small as typically seen in late-type spirals.

In order to evaluate whether the S0s are stripped spirals, the following picture can be outlined:

- (a) The parameters of the bulges and disks for the S0s in the NIRS0S sample are correlated, in a similar manner as for the spirals in the OSUBSGS sample, supporting the view that the *formation processes of bulges and disks in these galaxies are coupled*. This is expected if the disks were formed first and the bulges emerged from the disks by secular evolution.
- (b) *The properties of bulges in S0s are fundamentally different from the elliptical galaxies*. This is the case not only for

the bright S0s, but also for the faintest bulges, comparable in size with the dwarf ellipticals (dEs), which implies that the S0s are not likely to be the progenitors of dEs. On the other hand, the *bulges and disks of S0s are similar to those in S0/a–Scd spirals having bulges brighter than ~ -20 mag in K_s -band*, which is compatible with the idea that S0s are stripped spirals.

(c) *The bulges of a large majority of disk galaxies were formed by star formation in the disk.* This view is consistent with the above two points, and is supported by the obtained ratio r_{eff}/h_r^0 for S0s and spirals: the obtained small values are not easily compatible with the predictions of simulations in which bulges were formed by galaxy mergers.

(d) *Spiral galaxies with bulges brighter than $M_K^0 \sim -20$ mag, can be transformed into S0s by stripping the disk gas, followed by truncated star formation.* If star formation of the disk in spiral galaxies were truncated 1-6 Gyrs ago (see Begregal, Aragón-Salamanca & Merrifield 2006), it could explain the observed magnitude difference of ~ 1 mag in the disk luminosity between S0s and spirals (see our Fig. 11). Spiral galaxies which can evolve into S0s depends largely on the galaxy luminosity, and therefore also on the luminosity of the bulge, and not on the spiral Hubble type.

This scenario, where even late-type spirals could be progenitors of S0s, reminds of the early ideas by van den Bergh (1976, 1998; see also Sandage 2005), who suggested that spirals and S0s are spread throughout the Hubble classification scheme in parallel tuning forks (S0_a, S0_b and S0_c). The S0 galaxies studied by van den Bergh were fainter than the Sa spirals. Therefore he suggested that those S0s with small B/T flux ratios are “anemic” Sb and Sc galaxies, stripped of gas, which leaves only a bulge and a featureless disk. However, at that time no such galaxies were found. The S0 galaxies we study are not “anemic”, they are not fainter than the early-type spirals. For a representative sample of disk galaxies the K -band luminosities of S0s and spirals was studied recently by Burstein et al. (2005), showing that S0s and spirals have similar total luminosities. Taking into account that fading of star formation should lower the luminosity of S0s, this was considered as a problem for the stripping scenario. But, on the other hand, increase in the bulge luminosity due to internal dynamical effects might partly compensate the loss of the disk luminosity in S0s. Also, as shown in Figure 11, bright spirals might more easily transform into S0s. Moreover the disks in most S0 galaxies are not featureless: bars are known to be prominent in S0s, nuclear bars are frequent (Erwin & Sparke 2002; Laine et al. 2002; Laurikainen et al. 2009), and even a large majority of non-barred S0s have ovals or lenses (Laurikainen et al. 2009). The large number of bars, rings and lenses in the early-type galaxies is again consistent with the idea that S0s were stripped spirals. Otherwise it would be difficult to understand why these galaxies, deficient of gas, which should make the disk stable, have formed such frequently observed, prominent sub-structures in their disks.

The original idea of S0s as stripped spirals where star formation has ceased comes from the observation by Dressler (1980), who showed that S0s are common in nearby clusters, whereas spirals are more common in distant clusters. This has been recently re-investigated for the cluster Cl0024+16 at redshift $z=0.39$ by Moran et al. (2007). They found a large abundance of passive spirals (with only a small amount of HI gas and a low level of star formation), which were interpreted as galaxies in a transition state from spirals to S0s. The number of these galaxies was estimated to be large enough to explain the fraction of S0s in the nearby clusters. It was suggested by Moran et al. (2007) that the processes to form “passive” spirals in a low density interstellar medium could be ram pressure stripping, and in a more dense environment, galaxy interactions, starvation, and gentle stripping of the disks. However, it has been questioned whether typical spiral galaxy luminosities are sufficient to build up the brightest S0s in local clusters (Poggianti et al. 1999; Gerken et al. 2004). A natural solution for this problem comes from the recent study of luminous infrared galaxies (LIRGs) by Geach et al. (2009), who used 24 μ m band Spitzer observations. They showed that the LIRGs at $z\sim 0.5$ can account for the star formation needed to explain the bright end of the S0 luminosity function. These galaxies have morphological types of Sab, indicating that the bulges in the most massive S0s might form already at a fairly early stage of galaxy evolution. Based on an analysis of colors, Domínguez-Palmero & Balcells (2009) obtained a similar conclusion.

There is also other evidence supporting the view that S0s are stripped spirals. If interactions of galaxies with the intra-cluster medium, e.g., gas stripping, are responsible for the transformation of spirals into S0s, the number of globular clusters in these galaxies will not be affected. Indeed, this is what was found by Aragón-Salamanca, Bedregal & Merrifield (2006) and Barr et al. (2007). Results for the Tully-Fisher (Luminosity vs maximum rotation velocity) relation hint in the same direction: Bedregal, Aragón-Salamanca & Merrifield (2006) explained the location of the S0 galaxies below the spirals (lower L for a given V_{max}) arising from the luminosity evolution of spiral galaxies, in which star formation is ceased. The transformation was assumed to occur over a range of timescales, with the galaxies passively fading in the latest stage of the evolution. This is consistent with the results obtained in this study.

8 CONCLUSIONS

New 2D multi-component decompositions are presented for 122 early-type disk galaxies, as part of the Near-IR Survey S0 galaxy Survey (NIRS0S), using deep K_s -band images. Combined with our previous decompositions, this leads to a sample of 175 galaxies (117 S0s + 22 S0/a and 36 Sa galaxies). Of these galaxies, reliable decompositions could be made for 160 galaxies.

As a comparison sample we use the Ohio State University Bright Spiral Galaxy Sample (OSUBSGS) of spirals, for which similar multi-component decompositions have previously been made by us. Particular attention has been paid on correcting the effects of dust on the parameters of the bulges and disks. In our multi-component approach, 2D light distributions of galaxies are decomposed to structure components including, besides bulge and disk, also bars, ovals and lenses, using either Sérsic or Ferrers model functions. To our knowledge, this is a first attempt to study the scaling relations for a representative sample of S0s and spirals, applying the same multi-component decomposition approach for all galaxies.

Our main conclusions are the following:

(1) The photometric properties derived for the NIRS0S and the OSUBSGS samples show that the bulges of S0 galaxies are more tightly related to bulges of spirals than to elliptical galaxies. This is manifested in the $M_K^o(bulge)$ vs r_{eff} diagram, in the photometric plane, and in the Kormendy relation (Figs. 8a, 3, and 2, respectively). However, the brightest bulges among the S0-Sa galaxies in the Kormendy relation are located in the same region as the elliptical galaxies.

(2) The bulges in S0s are different from the elliptical galaxies. This is the case, not only for the bright galaxies, but also for those with sizes similar to the dwarf elliptical galaxies (S0s have several magnitudes higher surface brightnesses than dEs). This suggests that S0s are not likely to evolve into dwarf galaxies by galaxy harassment. On the other hand, the bulges of S0s are fairly similar to those of spirals having $M_K^o(bulge) < -20$ mag, except that they are slightly more compact (Fig. 8a) and do not show a statistically significant correlation between $M_K^o(bulge)$ and the Sérsic index n (Fig. 6a).

(3) The properties of bulges and disks of S0s in the NIRS0S sample are coupled, in a similar manner as has been found previously for spirals. This is manifested in the $M_K^o(bulge)$ vs $M_K^o(disk)$ (Fig. 11), $M_K^o(bulge)$ vs r_{eff} (Fig. 8a), as well as in the r_{eff} vs h_r^o diagrams (Fig. 10). For r_{eff} vs h_r^o we confirm previous results.

(4) We obtained median $r_{eff}/h_r^o = 0.20, 0.15$ and 0.10 for S0, S0/a and Sab-Sc galaxies, respectively. These values are a factor of ~ 2 smaller than obtained previously in the literature. Compared to the model predictions by Naab & Trujillo (2006), these values are not well compatible with the idea that the bulges of disk galaxies were formed by galaxy mergers, not even for S0s.

(5) The properties of the disks are very similar among the S0s and spirals: they occupy the same regions in the (a) h_r^o vs $M_K^o(disk)$, (b) μ_o vs $M_K^o(disk)$, and (c) μ_o vs h_r^o (Figs. 9a,b,c, respectively) diagrams. For both types of galaxies μ_o varies by 4.5 mag and the range in h_r^o is 1-10 kpc, in agreement with that obtained by GW2008 for spirals.

(6) The bulge-to-total flux ratio, B/T , for S0s covers the full range of $B/T < 0.7$ found in the Hubble sequence. Even 13% (N=12) have $B/T < 0.15$, typically seen in late-type spirals.

Our results support the view according that spiral galaxies with bulges brighter than -20 mag in K_s -band, can evolve directly into S0s by stripping the gas from the disk, followed by truncated star formation. This is estimated to be the case up to $\sim 50\%$ of the Sc-Scd type spirals. This view is consistent with the obtained scaling relations and the properties of bulges and disks of S0s and spirals, as discussed in our study.

ACKNOWLEDGMENTS

We thank the anonymous referee of careful reading of the manuscript, and Dr Alister Graham for constructive criticism. We acknowledge the time allocation committees of the NTT (074.B-0290(A), 077.A-0356(A), 081.B-0350(A)), WHT, TNG, NOT and KPNO telescopes for giving a significant number of observing nights for this project. The New Technology Telescope (NTT) is operated at the European Southern Observatory (ESO) in Chile. The William Herschel Telescope (WHT), the Italian Telescopio Nazionale Galileo (TNG), and the Nordic Optical Telescope (NOT), are operated on the island of La Palma by the Isaac Newton Group, the Fundacion Galileo Galilei of the INAF (Istituto Nazionale di Astrofisica), and jointly by Denmark, Finland, Iceland, Norway, and Sweden, respectively, in the Spanish Observatorio del Roque de los Muchachos of the Instituto de Astrofisica de Canarias. This publication makes use of data products from the Two Micron All Sky Survey, which is a joint project of the University of Massachusetts and the Infrared Processing and Analysis Center/California Institute of Technology, funded by the National Aeronautics and Space Administration and the National Science Foundation. It also uses the NASA/IPAC Extragalactic Database (NED), operated by the Jet Propulsion Laboratory in Caltech. EL and HS acknowledge the Academy of Finland of significant financial support. RB acknowledge the support of NSF grant AST-0507140. JHK acknowledges support by the Instituto de Astrofísica de Canarias (3I2407).

REFERENCES

- Aguerri J.A.L., Balcells M., Peletier R.F., 2001, AA, 367, 428
Aguerri J.A.L., Elias-Rosa N., Corsini E., Muñoz-Tuñón C., 2005a, AJ, 434, 109
Aguerri, J. A. L., Iglesias-Páramo, J., Vilchez, J. M., Muñoz-Tuñón, C., Sánchez-Janssen, R., 2005b, AJ, 130, 475

- Aguerri, J. A. L.; González-García, A. C., 2009, AA, 494, 891
- Andredakis Y. C., Sanders R. H, 1994, MNRAS, 267, 283
- Andredakis Y.C., Peletier R.F., Balcells M., 1995, MNRAS, 275, 874
- Aragón-Salamanca A., Bedregal A.G., Merrifield M.R., 2006, AA, 458, 101
- Athanassoula E., Misiortis A., 2002, MNRAS, 330, 35
- Athanassoula E., Lambert J.C., Dehnen W., 2005, MNRAS, 363, 496
- Balcells M., Graham A. W., Domínguez-Palmero L., Peletier R.F., 2003, ApJ, 582, 79
- Balcells M., Graham A.W., Peletier R.F., 2007, ApJ, 665, 1104
- Barnes, J.E., Hernquist L., 1992, ARA&A, 30, 705
- Barr, J.M., Bedregal A.G., Aragón-Salamanca A., Merrifield M.R., Bamford S.P., 2007, AA, 470, 173
- Bedregal A., Aragón-Salamanca A., Merrifield M., 2006, MNRAS, 373, 1125
- Bekki K., Couch W.J., Shioya Y., 2002, ApJ, 577, 651
- van den Bergh S., 1976, ApJ, 206, 883
- van den Bergh S., 1998, "Galaxy Morphology and Classification". Cambridge, Cambridge Univ. Press
- van den Bergh S., 2009, ApJ, 694, 120
- Bournaud F., Combes F., 2002, AA, 392, 83
- Bournaud F., Combes F., Semelin B., 2005, MNRAS, 364, 18
- Burstein D., 1979, ApJ, 234, 829
- Burstein D., Ho, L. C., Huchra, J. P., Macri, L. M., 2005, ApJ, 621, 246
- Buta R., Laurikainen E., Salo H., Block D. L., Knapen J. H., 2006, AJ, 132, 1859
- Buta R., Corwin H., Odewahn S., 2007, "The de Vaucouleurs Atlas of Galaxies", Cambridge, Cambridge University Press (BCO)
- Burkert A., Naab T., Johansson P.H., Roland J., 2008, ApJ, 685, 897
- Cameron E., Driver S. P., Graham A. W., Liske J., 2009, ApJ, 699, 105
- Caon N., Capaccioli M., D'Onofrio M., 1993, MNRAS, 265, 1013
- Capaccioli M., Caon, N., 1991, MNRAS, 248, 523
- Capaccioli M., Caon N., D'Onofrio M., 1992, MNRAS, 259, 323
- Cardelli J.A., Clayton G.C., Mathis, J.S., 1989, ApJ, 345, 245
- Cappellari, M. et al., 2007, MNRAS, 379, 418
- Carollo C. M., Stiavelli M., de Zeeuw P. T., Mack J., 1997, AJ, 491, 434
- Carollo C. M., Stiavelli M., 1998, AJ, 115, 2306
- Carollo C.M., Scarlata C., Stiavelli M., Wyse R.F.G., Mayer L., 2007, ApJ, 658, 960
- Courteau, S., de Jong R. S., Broeils A.H., 1996, ApJL, 457, 73
- Dalcanton, J. J., Spergel, D. N., Summers, F. J., 1997, ApJ, 482, 659
- Debatista V.P., Mayer L. Carollo C.M., Moore B. Wadsley J., Quinn T., 2006, ApJ, 645, 209
- Djorgovski S., Davis M., 1987, ApJ, 313, 59
- Domínguez-Palmero, L., Balcells M., 2009, ApJ, 694, 69
- D'Onghia E., Burkert A., Murante G., Khochfar S., 2006, MNRAS, 372, 1525
- Dressler A., 1980, ApJ, 236, 351
- Dressler A., Lynden-Bell D., Burstein D., Davies R.L., Faber S.M., Terlevich R., Wegner G., 1987, ApJ, 313, 42
- Driver, S. P., Allen, P. D., Graham, A. W., Cameron, E., Liske, J., Ellis, S. C., Cross, N. J. G., de Propris, R., P., S., Couch, W. J., 2006, MNRAS, 368, 414
- Driver S.P., Popescu C.C., Tuffs R. J., Graham A. W., Liske J., Baldry I., 2008, ApJ, 678, L101
- Eliche-Moral M.C., Balcells M., Aguerri J.A.L., González-García A.C., 2006, AA, 457, 91
- Erwin P., Sparke, L.S., 2002, AJ, 124, 65
- Erwin P., Beltrán, J.C.V., Graham A.W., Beckman J.E., 2003, ApJ, 597, 929
- Erwin P., 2004, AA, 415, 941
- Erwin P., Beckman J.E., Pohlen M., 2005, ApJ, 626, 81
- Eskridge P.B. et al., 2002, ApJS, 143, 73
- Freeman K.C., 1970, ApJ, 160, 811
- Firmani C., Avila-Reese V., 2000 MNRAS, 315, 457
- Fisher D., Franx M., Illingworth G., 1996, ApJ, 459, 110
- Gadotti D., 2008, MNRAS, 384, 420
- Geach J.E., Smail I., Moran S.M., Treu T., Ellis R., 2009, ApJ, 691, 783
- Gerken B., Ziegler B., Balogh M., Gijbank D., Friz A., Jager K., 2004, AA, 421, 59
- Graham A., Prieto M., 1999, ApJSS, 269, 653
- Graham A., 2001a, MNRAS, 326, 543

- Graham A., 2001b, AJ, 121, 820
Graham A., de Blok W.J., 2001, ApJ, 556, 177
Graham A., 2002, MNRAS, 334, 859
Graham A., Worley C.C., 2008, MNRAS, 388, 1708 (GW2008)
Gunn J.E., Gott J.R., 1972, ApJ, 176, 1
Hubble E., 1926, ApJ, 64, 321
Hunt L.K., Pierini D., Giovanardi C., 2004, AA, 414, 905
Illingworth, G. 1981, in “The structure and evolution of normal galaxies”, Proceedings of the Advanced Study Institute, Cambridge, England, August 3-15, 1980. (A82-11951 02-90) Cambridge and New York, Cambridge University Press, 1981, p. 27-41.
de Jong R.S., 1996, AA, 313, 45
Kauffmann G., Golberg J., Diaferio A., White S., 1999, MNRAS, 303, 188
Kautsch S.J., Grebel E.K., Barazza F D., Gallagher J.S., 2006, AA, 445, 765
Kent S.M., 1985, ApJS, 59, 115
Khochfar S., Burkert A., 2005, MNRAS, 359, 1319
Khochfar S., Silk J., 2006, MNRAS, 370, 902
Khosroshahi H., Wadadekar Y., Kembhavi A., 2000, ApJ, 533, 162
Khosroshahi H., Wadadekar Y., Kembhavi A., Mobasher, B., 2000, ApJL, 531, 103
Khosroshahi H., Raychaudhury, S., Ponman T.J. et al., 2004, MNRAS, 349, 527
Kodaira K., Watanabe M., Okamura S., 1986, ApJS, 62, 703
Kormendy J., 1977, ApJ, 218, 333
Kormendy J., 1979, ApJ, 227, 714
Kormendy J., 1982, ApJ, 257, 75
Kormendy J., 1984, ApJ, 286, 116
Kormendy J., Kennicutt R., 2004, ARA&A, 42, 603
Laine S., Shlosman I., Knapen J.H., Peletier, Reynier F., 2002, ApJ, 567, 97
Laurikainen E., Salo H., 2000, AA, 141, 103
Laurikainen E., Salo H., Buta R., Vasylyev S. 2004 MNRAS, 355, 1251
Laurikainen E., Salo H., Buta R., 2005, MNRAS, 362, 1319
Laurikainen E., Salo H., Buta R., Knapen J. H., Speltinckx T., Block D., 2006, AJ, 132, 2634
Laurikainen E., Salo H., Buta R., Knapen J. H., 2007, MNRAS, 381, 401
Laurikainen E., Salo H., Buta R., Knapen J. H., 2009, ApJL, 692, L34
Lisker T., Grebel E. K., Binggeli B., 2006, AJ, 132, 497
MacArthur L.A., Courteau S., Holtzman J.A., 2003, ApJ, 582, 689
MacArthur L.A., Courteau, S., Bell, E., Holtzman, J.A., 2004, ApJS, 152, 175
MacArthur L.A., Ellis R.S., Treu T.U, Vivian U., Bundy K. Moran S., 2008, ApJ, 680, 70
Mastropietro C., Moore B., Mayer L., Debattista V. P., Piffaretti R., Stadel J., 2005, MNRAS, 364, 607
Méndez-Abreu J., Aguerri J.A.L., Corsini E.M., Simonneau E., 2008, AA, 487, 555
Richard R., Marchal J., 1994, AAS, 105, 481
Moran S.M., Loh B.L., Ellis R.S., Treu T., Bundy K., MacArthur L.A., 2007, ApJ, 665, 1067
Moore B., Katz N., Lake G., Dressler A., Oemler A., 1996, Nature, 379, 613
Möllenhoff C., Heidt J., 2001, AA, 368, 16
Naab T., Burkert A., Hernquist L., 1999, ApJ, 523, 133
Naab T., Burkert A., 2003, ApJ, 523, 133
Naab T., Trujillo I., 2006, MNRAS, 369, 625
Naab T., Khochfar S., Burkert A., 2006, ApJ, 636, 81
Naab T., Ostriker J.P., 2009, ApJ, 690, 1452
di Nino D., Trenti M., Stiavelli M., Carollo C. M., Scarlata C., Wyse R. F. G., 2009, AJ, 138, 1296
Noordermeer E., van der Hulst J.M., 2007, MNRAS, 376, 1480
Pahre M.A., Djorgovski S., de Carvalho R.R., 1998, AJ, 116, 1591
Peletier R. F., Balcells M., 1996, AJ, 111, 2238
Peng, C. 2002, AJ, 124, 294
Pierini D., Gavazzi G., Franzetti P., Scodeggio M., Boselli A., 2002, MNRAS, 332, 422
Poggianti, B.M., Smail I., Dressler A., Couch W.J., Barger W.J., Butcher H., Ellis R.C., Oemler A.J., 1999, ApJ, 518, 576
Prieto M., Gottesman S.T., Aguerri J.L., Varela A.M., Munoz-Tunon C., 1997, AJ, 114, 1413
Prieto M., Aguerri J.L., Varela A.M., Munoz-Tunon C., 2001, AA, 367, 405
Ravikumar C.D., Barway S., Kembhavi A., Mobasher B., Kuriakose V.C., 2006, AA, 446, 827

- Reese A.S., Williams T.B., Sellwood J.A., Barnes E.I., Powell B.A., 2007, *AJ*, 133, 2846
- Salo H., Laurikainen E., Buta R., Knapen J.H., 2009 (SLBK, in preparation)
- Sandage A., 1961, "Hubble Atlas of Galaxies", Washington, DC: Carnegie Inst. Wash.Publ. 618
- Sandage A. R., Tammann G.A., 1981, "Revised Shapley Ames Catalog of Bright Galaxies", Carnegie Institute of Washington (RSA)
- Sandage A., Bingelli B., 1984, *AJ*, 89, 919
- Sandage A., 2005, *ARA&A*, 43, 581
- Sandage A., Bedke J., 1994, "The Carnegie Atlas of Galaxies". Washington, DC: The Carnegie Inst. Washington (CAG)
- Sarzi, M.; Allard, E. L.; Knapen, J. H.; Mazzuca, L. M., 2007, *MNRAS*, 380, 949
- Scannapieco C., Tissera P.B., 2003, *MNRAS*, 338, 880
- Schlegel D.J., Finkbeiner D.P., Davis M., 1998, *MNRAS*, *ApJ*, 500, 525
- Scodeggio M., Giovanelli R., Haynes M.P., 1997, *AJ*, 113, 2087
- Sérsic J.L., 1963, in *Boletín de la Asociación Argentina de Astronomía*, vol. 6, p.41
- Sérsic J.L., 1968, in *Atlas de Galaxias Australes* (Cordoba: Observatorio Astronomico)
- Skrutskie M.F., Cutri R.M., Stiening R., Weinberg M.D., Schneider S., Carpenter J.M., Beichman C., Capps R., Chester T., Elias J., and 21 coauthors, 2006, *AJ*, 131, 1163
- Somerville R.S., Primack J.R., 1999, *MNRAS*, 310, 1087
- Springel V., Hernquist L., 2005, *ApJ*, 622, L9
- Steinmetz M., Navarro J.F., 2002, *NewA*, 7, 155
- Trujillo I., Asensio Ramos A., Rubino-Martín J.A., Graham A.W., Aguerri J.A.L., Cepa J., Gutiérrez C. M., 2002, *MNRAS*, 333, 510
- Tsikoudi V., 1980, *ApJS*, 43, 365
- Tully R.B., 1988, "The Nearly Galaxy Catalog", Cambridge University Press
- Turnbull A.J., Bridges T.J., Carter D., 1999, *MNRAS*, 307, 967
- de Vaucouleurs G., 1959, in *Handbuch der Physik*, Volume 53, p.275
- de Vaucouleurs G., de Vaucouleurs A., Corwin H.G., 1976, *Second Reference Catalogue of Bright Galaxies*, 1976, Austin, University of Texas press
- de Vaucouleurs G., de Vaucouleurs A., Corwin H.G. Jr., Buta R., Paturel G., Fouque P., 1991, *Third Reference Catalogue of Bright Galaxies*, New York, Springer (RC3)
- Weil M. L., Hernquist L., 1996, *ApJ*, 460, 101
- Weinzirl T., Jogee S., Khockfar S., Burkert A., Kormendy J., 2009, *ApJ*, 696, 411
- Yoshizawa M., Wakamatsu K., 1975, *AA*, 44, 363
- Younger J.D., Cox T.J., Seth A.C., Hernquist L., 2007, *ApJ*, 670, 269
- de Zeeuw T., Franx M., 1991, *ARA&A*, 29, 239

APPENDIX A: DISCUSSION OF THE DECOMPOSITIONS FOR THE INDIVIDUAL GALAXIES

In the following decompositions for individual NIRS0S galaxies are discussed. It is done (1) if the solution is uncertain, (2) it was complicated to find, (3) the galaxy has a bar although it is not classified as a barred galaxy in RC3, or (4) the catalogued Hubble type needs revision. For 15 of the 176 galaxies no decomposition was made, either because the inclination was higher than 65° (NGC 2549, NGC 4220, NGC 4293, NGC 4429, NGC 5308, NGC 5448, NGC 5838, NGC 7332), the galaxy formed a strongly interacting pair (NGC 4105, NGC 6438, NGC 3718, NGC 5353), the image was not deep enough for detecting the exponential disk (NGC 6482), the galaxy had practically no bulge (IC 5240), or the decomposition was otherwise uncertain (NGC 3900). Weak bars detected in the residual images are discussed, but they are shown in the data-paper (SLBK) where all the structural components for the sample galaxies are illustrated.

IC 4329: The galaxy has a very dispersed bar-like structure ending up to a faint lens at the same radial distance ($\sim 55''$). Inside the bar there is a similar bar/lens structure at $r < 25''$ appearing also as an exponential subsection in the surface brightness profile. The two bar/lens components are visible also in the ellipticity profile. In the decomposition the inner bar/lens was fitted by a Ferrers function.

IC 4889: The galaxy is an elliptical galaxy in RC3 but, as noticed by Sandage & Bedge in CAG, it has a developed outer envelope which makes a classification to S0 justified. The inner parts of the galaxy also show isophotes that deviate from the outer disk. A weak lens was added to the decomposition, but it does not affect the parameters of the bulge.

IC 5267: In the near-IR this galaxy looks like typical S0 with two bright lenses with nearly circular isophotes, and a faint outer disk. In the decomposition the lenses were fitted by two Ferrers functions. However, in blue light it is classified as S0/a having also a partial outer ring.

IC 5328: This galaxy is classified as an elliptical galaxy in RC3, and as an S0 in RCA and in CAG. We first tried to use a single Sérsic function, but it failed to model the surface brightness profile properly. As the galaxy obviously has a lens, a Ferrers function was added, which considerably improved the fit: the solution converged even when leaving all the parameters of the bulge and the disk free for fitting. The residual image, after subtracting the bulge model, shows a very weak bar. There is no doubt that this is not an elliptical galaxy.

ESO 137-G10: In the K_s -band image the galaxy image looks featureless. Our best fitting model includes a fairly exponential bulge and an exponential disk. In the residual image, after subtracting the bulge mode, a faint lens is visible, detected also in CAG in the optical region.

ESO 337-G10: A simple bulge/disk decomposition was a good fit to the surface brightness profile, but it left a residual image where a lens was visible.

NGC 439: This galaxy is classified as SAB0⁻(rs) in RC3, and as E5 in CAG. Our K_s -band image shows no sign of a bar. In fact, the galaxy looks featureless and the two-dimensional surface brightness profile can be satisfactorily fitted by a single Sérsic function, supporting the GAC classification.

NGC 474: The galaxy has a weak oval bar surrounded by a lens with circular isophotes, each of which was fitted with a Ferrers function. The disk is exponential and shows some arc-like structures. These arcs have been interpreted as merger-created shells, possibly also influenced by the neighbor NGC 470 (Turnbull, Bridges & Carter 1999).

NGC 484: This galaxy is classified non-barred in RC3 and at first sight it indeed looks featureless. But, it has an elongated central component, most probably a bar, surrounded by a nuclear ring. The galaxy has also a weak lens extending to a large radial distance. However, these components are too weak for taking into account in the decomposition. We find two possible solutions, one obtained with a single Sérsic function, and another using a bulge-disk model. However, as a bar and a lens are visible in the residual image in the single function solution, the bulge-disk model was considered more reliable.

NGC 507: NGC 507 is reported to be a non-barred galaxy in all previous studies, but our K_s -band image shows a weak bar in the unsharp mask image (see SLBK). The bar is too weak to be fitted in the decomposition, but as it is surrounded by a bright oval, we can fit both components with a single Ferrers function.

NGC 524: This galaxy is a typical example of a non-barred S0: the surface brightness profile shows two lenses, which are directly visible also in the image. By adding two Ferrers functions with $n = 1$ gives a good fit to the observed flux distribution. A comparison with a deep optical image also shows that the component fitted as an exponential disk is actually a third lens (see SLBK).

NGC 584: Although an elliptical in RC3, we classify this galaxy as an S0, which is also in agreement with Buta, Corwin & Odewahn (2007, hereafter BCO). It has a bright central oval and a weak bar inside the oval. The surface brightness profile shows an intermediate region between the bulge and the disk. In our decomposition we fitted the bar/lens using a single Ferrers function.

NGC 890: In RC3 this galaxy belongs to the family class AB. However, there is no clear evidence of a bar in the K_s -band image. However, the galaxy has boxy isophotes at $r < 10''$. In the decomposition a Ferrers function was fitted to this boxy component. By excluding it a boxy oval appears in the residual image, after subtracting the bulge model from the original image. However, the oval does not affect the parameters of the bulge or the disk.

NGC 1161: This galaxy is classified as non-barred S0 in RC3 and by BCO, but it shows a weak bar in the residual image after subtracting the bulge model from the original image. We tried first a simple bulge/disk decomposition which gives a quite good fit. However, by including a Ferrers function for the bar, less structure appeared in the residual image.

NGC 1201: This is again a non-barred galaxy in RC3, but our K_s -band image shows two bars. The secondary bar is also surrounded by an oval. In our best fitting model the two bars were fitted by Ferrers functions: for the secondary bar and the oval a single function was used. The different structure components were found iteratively in small steps. The final solution was maintained even after leaving all the key parameters free for fitting.

NGC 1302: This galaxy has a nearly round bulge and a bar surrounded by a lens. The bar and the lens were fitted separately. If all the parameters were left free for fitting, the flux of the bulge, the lens, and the bar were degenerated, which was possible to see in the model image. A decomposition for this galaxy has been previously made also by Laurikainen et al. (2004) using the OSUBSGS H -band image, leading to a higher B/T flux-ratio than obtained in this study ($B/T = 0.40$, and 0.25 , respectively). This difference can be explained by the fairly bright lens included to the decomposition in this study, but not by Laurikainen et al.

NGC 1344: The galaxy is classified as E5 in RC3, but in our classification it is an S0. To the decomposition we included an oval, fitted with a Ferrers function.

NGC 1351: As the surface brightness profile shows an exponential disk and a prominent bulge, we started with a bulge/disk decomposition. However, after subtracting the bulge model from the original image a weak bar appears in the residual image. In the final decomposition a Ferrers function was used for the bar. However, the bar is so weak that it does not affect the parameters of the bulge or the disk.

NGC 1371: The galaxy has a weak bar with some characteristics of spiral arms. In the decomposition this component was fitted with a Ferrers function. The spiral arms seem to be forming an inner ring.

NGC 1380: The galaxy has a weak bar with ansae at the two edges. In the central parts of the galaxy there is either a flattened bulge or an oval.

NGC 1389: The galaxy has a small bar oriented along the main disk (visible in the direct image). The bar is surrounded by a lens with a different orientation. In the decomposition the lens was fitted by a Ferrers function, whereas the bar was too weak to be taken into account.

NGC 1537: The galaxy has a bar visible in the direct image, but it was too weak to be taken into account in the decomposition.

NGC 1543: This galaxy has two bars, a nearly circular lens surrounding the primary bar, and a prominent, broad and diffuse outer ring. The bulge is nearly spherical. The outer ring dominates the outer part of the disk. In the decomposition the two bars were fitted by Ferrers functions. The decomposition did not converge, but at the end the solution changed very little in the iterations. In order to avoid too long bar model the length was forced to 75 arcsec. At the beginning some flattening for the bulge was given, but in the iterations the bulge turned to spherical.

NGC 1617: The galaxy has a bar with some characteristics of spiral arms. It has also an outer ring, probably forming a lens. The bar and the lens/outer ring were fitted by Ferrers functions.

NGC 2217: The galaxy has two bars and a lens surrounding the primary bar. These components were fitted with three Ferrers functions. The secondary bar was fitted together with an oval surrounding it. Due to the oval, estimating the flattening of the bulge was not self-evident. However, using a nearly spherical bulge, a well-defined oval (similar to the observed one) in the model image was produced. The outer disk is dominated by an outer ring, which makes the scale length of the disk unreliable.

NGC 2300: This galaxy is classified as an S0, in RC3 and by Michard & Marchal (1994), whereas in CAG it is classified as an elliptical galaxy. The surface brightness profile shows clearly an exponential disk which confirms that the galaxy is an S0. It has also a nearly exponential subsection at $r < 20''$ associated to a lens, which is visible also in the direct image. The lens was fitted by a Ferrers function.

NGC 2655: This galaxy has a large flattened component and a faint, extended and non-regular outer envelope. In the decomposition we assumed that the flattened structure is a bulge. This led to an extremely large B/T flux-ratio ($B/T = 0.66$), which is consistent with the visual impression of the image and the surface brightness profile.

NGC 2685: NGC 2685 is classified as barred S0 in RC3. Ravikumar et al. (2006) have also detected an inner disk in the H -band using the Hubble Space Telescope. Our image shows that the galaxy has an oval-shaped component at $r < 50''$, oriented along the outer disk. This oval component can be either a bar ($\epsilon = 0.65$) or an inner disk. In our decomposition this component was fitted by a Ferrers function, whereas the inner disk was not considered.

NGC 2768: This galaxy is classified as E6 in RC3, and as an S0 in CAG and by BCO. Although the galaxy is fairly featureless, it has boxy isophotes at a large radial range. The surface brightness profile clearly shows an intermediate region between the bulge and the disk. In the decomposition we fitted an oval using a Ferrers function. Leaving the parameters of the oval free for fitting, the boxy isophotes were automatically found. Our best fitting model is good everywhere else except in the innermost pixels. This is because the galaxy has also a nuclear bar at $r < 2''$ (see SLBK), which was not possible to take into account in the decomposition.

NGC 2782: This galaxy has a small, dusty bar at $r < 7''$, and a complex lens-like structure outside the bar. In the decomposition only the flat component was possible to take into account (the bar is too weak and knotty). The decomposition did not converge, but the obtained solution looks reasonable.

NGC 2787: This galaxy has a bar and a bright lens or oval inside the bar, each of which was fitted with a Ferrers function ($n = 2$ and $n = 1$, respectively). The central regions of the image have nearly spherical isophotes. We made first a bulge/disk/bar decomposition, leaving all the key parameters free for fitting. This approach gave a fairly good fit to the surface brightness profile, but the model image was not comparable with the observed image. Adding an oval considerably improved the model image.

NGC 2902: This is again a prototypical S0 having a prominent lens, which is important to take into account in the decomposition. The galaxy has also a weak bar inside the lens, visible only in the residual image after subtracting the bulge model from the original image (see SLBK).

NGC 2950: This galaxy has two bars, both surrounded by a lens or an oval. The secondary bar and the surrounding oval were fitted by a single Ferrers function, whereas for the primary bar and the lens surrounding it two different functions were used. The decomposition was started by finding the parameters of the disk, which were fixed at the beginning. After that a bulge/disk/bar decomposition was made, and finally the rest of the components were added to the fit iteratively. Once all the structure components were found, all parameters of the bulge and the flux of the other components, were left free for fitting. The solution did not converge, but at the end it changed extremely slowly. The found solution looks reasonable.

NGC 3032: The galaxy has two nearly circular lenses visible both in the direct image and in the surface brightness profile. In the decomposition they were fitted by Ferrers functions. It is possible that the exponential part of the surface brightness profile fitted as a disk, actually is a lens.

NGC 3166: This galaxy has three classical bars perpendicular to each other. The primary bar is surrounded by a nearly circular lens, and the secondary bar by another lens. The tertiary bar has boxy isophotes in the middle part of the bar. Unfortunately the FOV is too small for detecting the outer disk. In the decomposition we used three Ferrers functions: one for the primary bar, one for the lens surrounding it, and one for the secondary bar together with the surrounding lens. An exponential function was used to model the outer disk, including the tertiary bar. The components were found iteratively in small steps. In spite of the fact that the solution for the outer disk is only an approximation, the inner regions were possible to fit in a reasonable manner.

NGC 3169: In RC3 this is a non-barred galaxy, but our K_s -band image shows a weak bar at $r < 10''$. The bar is visible in the unsharp mask image (see SLBK). The image shows boxy isophotes at $r < 50''$, which might form part of a larger bar. However, both components are too weak to be taken into account in the decomposition.

NGC 3245: This galaxy has a small inner disk visible in the direct image, which might be related to a nuclear ring. It is surrounded by a bright lens or an oval, manifested as a broad bump in the surface brightness profile. In the decomposition the lens and the outer disk were fitted by a single exponential function, whereas the inner disk was fitted by a Ferrers function.

NGC 3358: The galaxy has a secondary bar and a primary bar surrounded by a weak lens. The outer disk is very flat and drops rapidly at the outer edge. The disk has also some spiral structure. In the decomposition it was possible to model the nuclear bar with one Ferrers function, and the primary bar, together with the surrounding lens, with another Ferrers function. The bulge is the small, nearly round component in the galaxy center. In this case there is no confusion with the bulge and the other components of the galaxy.

NGC3384: The image shows a bright, nearly round bulge, a weak bar, and an elongated central structure, most probably a nuclear bar. In our decomposition the two bars were fitted by Ferrers functions. This solution leads to a considerably smaller B/T flux-ratio than obtained previously by Fisher, Franx & Illingworth (1996) using a simple bulge/disk approach ($B/T = 0.32$ vs. 0.53 , respectively).

NGC 3414: In the CAG this galaxy is given as an example of an S0 having a very bright bulge and one of the faintest disk-to-halo (bulge) ratios seen in any disk galaxy. De Vaucouleurs et al. (1976) reports also a faint diffuse bar, but the bar has not been considered in more recent classifications of this galaxy. In our decomposition a bar was fitted by a Ferrers function. However, it is also possible that this is a galaxy seen nearly edge-on. For the uncertainty in the galaxy orientation the obtained solution should be considered with caution.

NGC 3489: In spite of its apparent simplicity this galaxy has actually a fairly complicated morphology (see SLBK): it has a weak bar inside a flattened bulge, and boxy isophotes outside the bar. In the decomposition the bar was fitted by a Ferrers function.

NGC 3516: This galaxy has a bar and a lens surrounding it. In the decomposition we used two Ferrers functions to fit these components. However, the interpretation of the bulge is not self-evident. The central regions of the galaxy are flattened and are assumed to be the bulge. However, based on the twisted isophotes in that region (see SLBK) it could be an oval as well. We consider the obtained B/T as an upper limit.

NGC 3607: This galaxy has a bright, nearly circular lens, and a slightly flattened bulge. The lens, fitted by a Ferrers function in the decomposition changes the B/T flux-ratio from 0.31 to 0.36 , and the Sérsic index from $n = 1.5$ to $n = 1.6$.

NGC 3665: NGC 3665 has a flattened bulge or an oval, as well as inner and outer disks. However, the inner disk is so weak that it cannot be taken into account in the decomposition. In the best fitting decomposition the flat inner component was interpreted as a bulge. We also tried whether a single Sérsic function is capable to fit the whole surface brightness profile, but that was not the case.

NGC 3729: This galaxy is dominated by a knotty central component, a bar and an inner ring. We made a bulge/disk/bar decomposition. The parameters of the bar were found first. After that the bar parameters, except for the flux, were fixed and the parameters of the bulge were found. In this approach a slightly flattened, extremely small bulge with $B/T = 0.03$ was found. The found extremely small B/T flux-ratio is not consistent with the Sa Hubble type given for this galaxy.

NGC 3892: The galaxy has a bright central component, and a diffuse bar ending up to a nearly spherical lens. Outside the lens a weak disk appears. In the decomposition two Ferrers functions were used to fit the bar and the lens. We first tried a bulge/disk/bar/lens decomposition, but it left a large residual to the central regions of the galaxy. The fit in the central regions was considerably improved by adding another Ferrers function representing another lens inside the bar. The obtained $B/T = 0.11$ is one of the smallest found for the S0 galaxies in our sample.

NGC 3945: This galaxy has a primary and a secondary bar, both surrounded by a lens. It has also an inner and an outer ring. In our decomposition different Ferrers functions were used to model the primary bar, the lens surrounding it, and the inner bar/lens system. The scale length of the disk, which for this galaxy is only an approximation, was found using the 1D-version of the code, by fitting an exponential function to the outer isophotes. The other components were found iteratively in small steps. At the end all the parameters of the bulge and the flux of the other components were left free for fitting.

NGC 3998: This is one of the clearest examples of lens dominated S0 galaxies in our sample. In the surface brightness profile an exponential sub-section at $r < 15''$ shows a bright lens. There is also a weak bump in the surface brightness profile at $r \sim 40''$, which hint to an outer lens. In the decomposition the bright inner lens was fitted with a Ferrers function. The exponential disk in the decomposition included also the outer lens, but the lens is not expected to significantly affect the parameters of the disk. This galaxy has a weak bar at $r < 8''$, which is visible in the residual image after subtracting the bulge model. A more detailed discussion of this galaxy is found in Laurikainen et al. (2009).

NGC 4138: This galaxy has an inner and an outer lens, the latter ending up to an inner ring. In our decomposition we fitted the inner lens, whereas the outer lens and the ring were included to the exponential disk. The bulge is so knotty

that this approximation is not expected to affect the parameters of the bulge. Excluding the lens in the decomposition barely affects the B/T flux-ratio ($B/T = 0.07$ and 0.11 , respectively), but it changes the Sérsic index from $n = 2.4$ to $n = 1.7$.

NGC 4203: This galaxy has a weak bar embedded in a bright oval, and an almost circular weak outer lens. The bar is well visible in the residual image after subtracting the bulge model (see SLBK). In the decomposition we fitted the inner lens and the bar with a single Ferrers function. The disk and the outer lens were included to the fit of the exponential disk.

NGC 4262: The galaxy has a bright, nearly spherical bulge, a bar, and a lens extending well outside the bar radius. We made a bulge/disk/bar decomposition, which showed the lens in the residual image, after subtracting the model image from the original image. However, the lens is so weak that it does not affect the parameters of the bulge or the disk. This galaxy is reported to have also an inner disk in the optical region (Erwin 2004), but it is not visible in our K_s -band image.

NGC 4314: NGC 4314 has a weak nuclear bar surrounded by a nuclear ring. It has also a strong primary bar and a fat inner component elongated along the thin bar, most probably being part of the bar itself. In the decomposition we used two Ferrers functions, one for the primary bar, and one for the nuclear bar/ring system. In the residual image, after subtracting the model from the original image, the fat bar component is visible. We tried to add also the fat bar component to the decomposition, but it disappeared in the iterations. We also tried a solution where some flattening was given to the initial bulge model, and the orientation of the bar, but it did not lead to a flat bulge model.

NGC 4369: This galaxy has a small bar surrounded by a lens, which again is surrounded by another lens. The surface brightness profile shows that the bulge and the bar have almost similar surface brightnesses. A bump in the surface brightness profile at $r = 10\text{--}15''$ corresponds to irregular spiral structure around the bar. In the decomposition we fitted the bar with a Ferrers function and the outer lens by an exponential function. No separate disk was fitted. However, due to the small number of pixels above the exponential part of the surface brightness profile, the obtained solution is highly uncertain. Most probably the B/T flux-ratio for this galaxy is extremely small.

NGC 4371: This galaxy has an ansae-type bar ending up to an inner ring. Inside the bar there is an inner disk and a nuclear ring. In the decomposition Ferrers functions were used to fit the bar and the inner disk/ring system. The bulge was forced to be spherical. If the ellipticity of the bulge was left free for fitting the bulge model would erroneously consist of the flux of the outer disk. These two models would give completely different B/T flux-ratios ($B/T = 0.19$ and 0.53 , respectively).

NGC 4373: This galaxy is classified as SAB0⁻ in RC3 and as an elliptical galaxy in CAG. In our K_s -band image the galaxy looks featureless, but the surface brightness distribution cannot be fitted well by a single Sérsic function. We then fitted a bulge and a disk: this model did not converge, but at the end the model changed extremely slowly. In the residual image (observed image - model image) a weak bar was visible.

NGC 4378: This is an Sa galaxy having faint, very tightly wound spiral arms. The arms seem to be forming two lens-like components. The weak disk is dominated by an outer pseudo-ring. In the decomposition we fitted the two lens-like components with Ferrers functions. These functions affected considerably the B/T flux ratio: while the simple bulge/disk decomposition gave $B/T = 0.54$, including the lenses gave $B/T = 0.31$.

NGC 4424: This galaxy has a very small bulge or no bulge at all. We give a bulge/disk/bar decomposition, but for the small number of pixels in the bulge, only the parameters of the disk are reliable. This is again one of the early-type galaxies that have a bulge, similar to those found in late-type galaxies.

NGC 4435: This galaxy has a bar with a boxy oval inside. We made a simple bulge/disk/bar decomposition, in which case the flux of the boxy oval goes to the bulge. However, the boxy oval might be a manifestation of a nuclear bar, for which reason the obtained B/T ratio can be considered as an upper limit.

NGC 4457: A dominant feature in this galaxy is a lens, which has a weak embedded bar. The outer disk is dominated by a weaker lens-like outer ring, whereas in the central regions there is a secondary bar surrounded by an oval. In the decomposition the secondary bar and the surrounding oval were fitted by a single Ferrers function. In the decomposition we fitted the primary bar/lens system with an exponential function and ignored the outer ring. This solution is expected to be only an approximation for the disk, but presumably does not significantly affect the parameters of the bulge.

NGC 4459: This galaxy has a bright, nearly round central region, and an exponential disk where also a lens appears. The lens is visible both in the direct image and in the surface brightness profile. In the decomposition it was fitted by a Ferrers function. A good solution was found using an image rebinned by a factor of 4, but a similar solution using the full resolution image did not converge. Therefore, in the final solution the number of iterations was limited.

NGC 4477: The galaxy has a classical bar surrounded by multiple shell-like or ring-like structures, which form part of an exponential disk. In the surface brightness profile the shell-like structures appear as flux slightly above the exponential light distribution. A good fit was obtained using a Ferrers function for the bar.

NGC 4531: This is a dwarf galaxy having a spiral-like bar embedded inside a lens. The surface brightness profile shows that the bulge is very small and has a low surface brightness. All the components of the disk were fitted by a single exponential function. A simple bulge/disk decomposition, leaving all the key parameters free for fitting, leads to an extremely large Sérsic index ($n = 5.3$). In this solution the bulge extends throughout the galaxy. We consider this solution unrealistic and find an other solution with a smaller bulge (shown in Fig. 1). It was found by selecting the initial parameters more carefully. We also limited the number of iterations otherwise, after a certain number of iterations, a sudden jump to the large bulge solution occurs.

NGC 4546: In our best fitting solution a bulge, a disk and a bar were fitted. The galaxy has also a weak secondary bar visible in the residual image, after subtracting the bulge model from the original image. The secondary bar appears also as a small peak in the ellipticity profile. However, it is not expected to affect the parameters of the bulge or the disk.

NGC 4612: The galaxy has a weak bar surrounded by a prominent lens. The outer disk is weak and it is dominated by an outer ring. In the decomposition we fitted the bar with a Ferrers function and the lens with a Sérsic function. Our best fitting decomposition looks a reasonable fit, but the solution did not converge. For this galaxy the bar affects the parameters of the bulge: a simple bulge/disk decomposition would considerably overestimate the flux of the bulge leading to $B/T = 0.63$ whereas the bulge/disk/bar/lens model gives $B/T = 0.21$. The Sérsic index in the two models also differ considerably ($n = 4.1$ and 2.2 , respectively). The image is not deep enough for obtaining the scale length of the disk in a reliable manner.

NGC 4694: The galaxy has a bright oval-like component and a peculiar nuclear bar or an inner disk. In the decomposition the central component was fitted by a nuclear exponential function.

NGC 4696: This galaxy is classified as an elliptical galaxy both in RC3 and in RSA, whereas in CAG it is S0₃(0) galaxy. We found that it is not possible to fit the 2D surface brightness profile by a single Sérsic function, thus supporting the S0 classification. The S0 nature is manifested also by several exponential subsections in the surface brightness profile, associated to lenses. Also, the outer part of the surface brightness profile is exponential.

NGC 4754: The galaxy has two bars, of which the secondary bar is embedded inside an oval. In the decomposition the bars were fitted by Ferrers functions.

NGC 4772: This galaxy is reported in the literature as an Sa galaxy in the optical (RC3, BCO, CAG), and as an S0 in the near-IR (Eskridge et al. 2002). The galaxy has a bright bulge surrounded by a disk, which might be seen nearly edge-on. It is surrounded by a faint outer disk.

NGC 4880: This galaxy has a very small bulge, a small peculiar bar, and a lens extending well outside the bar radius. In the decomposition the bar and the lens were fitted by two Ferrers functions. Due to the small number of pixels in the bulge model it is not considered to be uncertain.

NGC 4976: Again, a controversy exists in the classification given in RC3, where the galaxy is an elliptical, and in the CAG where it is classified as a prototypical S0₁. Indeed, the K_s -band surface brightness profile shows a deviation from a typical profile of an elliptical galaxy: the central region is too bright and also, the flux density does not decrease smoothly. As a confirmation check we tried to fit the 2D flux distribution with a single Sérsic function, but the model failed to fit the central regions of the galaxy. However, a good fit in the central regions was obtained by adding a Ferrers function, representing a lens, to the model. This component ($r \sim 17''$) can be associated also as a bump in the ellipticity profile (see SLBK).

NGC 4984: NGC 4984 has a primary and a secondary bar, both embedded inside lenses. In the decomposition the two bar+lens systems were fitted by Ferrers functions. While finding the parameters of the primary bar a series of decompositions were made until the model image looked similar to the observed image. The galaxy has a weak outer disk having also an outer ring, which makes the parameters of the disk somewhat uncertain.

NGC 5026: The galaxy has a bar surrounded by a weak lens, ending up to the the same radius with the bar. Spiral arms, forming an inner ring, also start from the two ends of the bar. A flattened bulge appears inside the bar. In our decomposition the bar was fitted by a Ferrers function, whereas the lens was not fitted. The exponential function for the outer disk is not perfect, because the disk is fairly flat. It is possible that the component fitted as an exponential disk is actually a lens.

NGC 5087: This galaxy is classified as an S0 both in RC3 and in CAG. The image shows a weak bar which was fitted by a Ferrers function.

NGC 5121: The galaxy has a bright, nearly circular bulge, a small central component, and a bright lens at $r < 40''$. The lens is manifested also as a broad bump in the surface brightness profile. The lens and the central elongated component were fitted by Ferrers functions.

NGC 5206: The galaxy has a bright nucleus and a very faint dispersed bar at $r < 80''$. The galaxy has also a faint circular component at $r < 15''$, which most probably is a lens. In the decomposition we fitted the nucleus with a Gaussian function, the bulge with a Sérsic function, and the bar with a Ferrers function. The lens was not modeled, but it is also so weak that it does not affect the decomposition. The found solution gives one of the smallest B/T flux-ratios ($B/T = 0.08$) for S0s.

NGC 5266: The galaxy has either a bright oval or a slightly flattened bulge, surrounded by a faint disk. The dust lane crossing the flattened component is visible in the K_s -band image. In the decomposition the flattened component was fitted by a Sérsic function and it was interpreted as a bulge. A single Sérsic function does not give a good fit to the surface brightness distribution.

NGC 5273: This galaxy has a nuclear bar and a lens extending to a much larger radius than the bar. In the decomposition only the lens was fitted. The bar is so weak that it does not affect the model.

NGC 5333: NGC 5333 has an oval-bar, having also an elongated inner component inside the bar, aligned nearly in the same orientation with the bar. These two components were fitted by Ferrers functions in the decomposition.

NGC 5365: This galaxy has a primary bar embedded in a weak lens, and a secondary bar embedded in a bright oval. The outermost structure in the image is probably also a lens ending up to an outer ring. This galaxy is discussed in detail by Laurikainen et al. (2009), where the image is also shown in different scales, demonstrating the different structure components. The primary bar and the lens were fitted by a single Ferrers function, whereas the nuclear bar and the oval were fitted by a single Sérsic's function. The outer part of the image was fitted by an exponential function.

NGC 5377: The galaxy has a strong bar with boxy or x-shaped isophotes inside the bar. The galaxy has also a nuclear bar. In the decomposition the two bars were fitted with Ferrers functions.

NGC 5419: This galaxy is classified as an elliptical galaxy in RC3, and as S0 in SGC and in CAG. The K_s -band surface brightness profile clearly shows an exponential disk, characteristic for S0s. There is also a lens, manifested in the in surface brightness profile. Also, the 2D flux distribution cannot be fitted by a single Sérsic function. The best fit was obtained with a three component model where a Ferrers function was used for the lens.

NGC 5473: This galaxy has a classical bar inside a bright oval. The bar/oval structure is embedded in a weak lens, oriented perpendicular to the oval. We made a simple bulge/disk/bar decomposition where a single Ferrers function was used for the bar/oval system. The lens was not fitted, but it is so weak that it does not affect the parameters of the bulge or the disk.

NGC 5485: The galaxy image looks fairly featureless, but more careful inspection shows a boxy oval or a lens, manifested also in the surface brightness profile. We made first a simple bulge/disk decomposition leaving all the key parameters free for fitting, but it left a lens in the residual image. In the final decomposition the oval was fitted by a Ferrers function.

NGC 5493: The galaxy has a long bar and also an inner elongated component along the bar. Due to its orientation it is most probably part of the bar. The bar was fitted by a Ferrers function.

NGC 5631: This galaxy looks fairly featureless, except that it has a lens, manifested both in the galaxy image and in the surface brightness profile. The outer disk looks exponential, but a comparison to an optical image shows that it is actually another lens (see SLBK). In the decomposition the lens was fitted by a Ferrers function, although it does not affect the parameters of the bulge.

NGC 5636: NGC 5636 is classified as an elliptical galaxy in RC3. However, the galaxy has an exponential surface brightness distribution at a large radial range, which hints to an S0. Also, a decomposition using a single de Vaucouleurs type Sérsic function did not work for this galaxy. Leaving all the parameters of the bulge and the disk free for fitting results to $B/T = 0.48$. A slightly smaller B/T flux-ratio of 0.41 is obtained by adding to the decomposition a lens. The decompositions with and without a lens give equally good fits.

NGC 5728: This galaxy has a primary and a secondary bar, both surrounded by a lens. The inner bar/lens system is also surrounded by a nuclear ring. In our decomposition we fitted the primary bar and the surrounding lens with two Ferrers functions, and the secondary bar/lens system with a third Ferrers function. The exponential disk is very weak so that h_r was found using the 1D-version of the code. In order to avoid degeneracy of the different components we started with a spherical

bulge and found the parameters of the two outer Ferrers functions first. These parameters were then fixed. After that the bulge (which was still assumed to be spherical) was fitted. Then the parameters of the nuclear component were found and finally, except for the flux, were fixed. At the end the key parameters of the bulge (including the flattening) were fitted together with the other components whose fluxes were left free for fitting.

NGC 5750: A prominent feature in this galaxy is the inner ring surrounding a weak bar. There is also an oval inside the bar. In our decomposition only the bar was fitted with a Ferrers function. The outer disk was found by fitting an exponential function to the surface brightness profile outside the ring, using the 1D-version of the code. The final 2D solution did not converge, but at the end it changed extremely slowly. Finally the number of iterations was limited.

NGC 5846: This galaxy has three lenses with nearly circular isophotes, the first showing as a bump in the surface brightness profile at $r < 4''$, whereas the other two are manifested as exponential sub-sections in the profile. The outermost lens at $r < 30''$ is obvious in the direct image, but is less clear in the surface brightness profile. In the decomposition all three lenses were fitted with flat Ferrers functions, although only the two inner lenses affected the bulge/disk solution.

NGC 5898: This galaxy, with its multiple lens structure, is again a prototypical S0 (see SLBK). We tried to fit the lenses that appear at $r = 7''$ and $20''$, but only the outer lens was maintained in the decomposition. We found that including it to the decomposition is important, otherwise we would have $B/T = 0.66$, instead of 0.44, and a Sérsic index 3.1 instead of 2.2.

NGC 5953: The galaxy has a nearly circular bulge, flocculent spiral arms in the inner part of the disk forming a lens, and a featureless outer disk. The lens appears as a bump in the surface brightness profile, and in the decomposition it was fitted by a flat Ferrers function. This galaxy also forms part of a closely interacting pair for which reason the decomposition was limited to a radial distance of $33''$. In the adopted portion of the surface brightness profile there is still some flux from the companion, visible above the exponential disk, but that is not expected to affect the scale length of the disk.

NGC 5982: NGC 5892 is again classified as an elliptical galaxy in RC3, which is consistent with the observation that it has shell-like structures in the K_s -band image. In our decomposition it was possible to fit the surface brightness profile both by a single Sérsic function, and using two Sérsic functions, where the inner component represents a small inner disk. We confirm that this galaxy is an elliptical galaxy.

NGC 6340, NGC 6407: These galaxies are non-barred systems, but have evidence of a prominent lens, manifested as exponential sub-section in the surface brightness profile. If a simple bulge/disk decomposition is made for these galaxies, and the bulge model subtracted from the original image, the lenses are clearly visible in the residual images.

NGC 6654: This galaxy is classified as a barred S0/a in RC3. It is a double barred system, the secondary bar being embedded inside a bright oval. In the decomposition both bars were fitted by Ferrers functions. For the secondary bar the bar model includes also the flux of the surrounding oval.

NGC 6684: This galaxy has a primary bar ending up to an inner ring, and a secondary bar embedded inside an oval. The scale length of the disk was found using the 1D-version of the code. In the final 2D decomposition both bars were fitted, using a single Ferrers function for the secondary bar and the surrounding oval. However, the nuclear bar+oval did not significantly affect the parameters of the bulge. The solution did not converge, but at the end changed very slowly. Finally the number of iterations were limited.

NGC 6703: This galaxy has two lenses, at $r = 20''$ and at $r = 45''$. In our decomposition we fitted only the inner lens, manifested as an exponential sub-section in the surface brightness profile. The outer lens is too weak to be taken into account in the decomposition.

NGC 6861: K_s -band image shows an elongated structure which can be an inner disk or a bar. Taking into account that it is oriented along the disk major axis, it is most probably a disk. In our decomposition it was fitted by a Sérsic function.

NGC 6958: In RC3 NGC 6958 is classified as an elliptical galaxy, but in CAG it appears as an S0. Based on the fact that the galaxy has an exponential outer disk and a prominent lens, manifested as an exponential sub-section in the surface brightness profile, the S0 classification is confirmed in this study.

NGC 7029: This galaxy has a bulge and an inner disk, surrounded by a boxy oval. Most probably there is an exponential disk outside the boxy oval, but the FOV of the image is too small to confirm that. For this galaxy we made a simple bulge/disk decomposition: we were not able to fit the inner disk, which disappeared during the iterations. However, the inner disk is so weak that it barely affects the parameters of the bulge. The obtained solution needs to be used critically, because the flux that

was fitted as an exponential disk actually corresponds the flux of the boxy oval. In the statistics we don't use the obtained parameters for the disk.

NGC 7049: This galaxy is classified as an S0 in RC3. We made a simple bulge/disk decomposition, which gave one of the highest B/T flux-ratios in our sample. It was not possible to fit the 2D surface brightness distribution by a single Sérsic function.

NGC 7079: NGC 7079 has a weak primary bar embedded in a lens, and an oval inside the bar. In the decomposition we fitted the bar and the lens with a single Ferrers function. We tried to fit also the oval, but it did not survive in the iterations. The slightly curved surface brightness profile at $r > 20''$ hints to the possibility that the section we call an exponential disk is probably an outer lens.

NGC 7192: This galaxy is dominated by two lenses, the inner lens manifested as an exponential sub-sections at $r = 10''-17''$ in the surface brightness profile, and the outer lens as a broad bump at $r = 17''-47''$. The outer disk is exponential. In the decomposition the 2D surface brightness distribution is well fitted using Ferrers functions for the lenses.

NGC 7213: This galaxy is again dominated by two lenses. The bright inner lens, which appears as a weak bump in the surface brightness profile at $r < 20''$, includes a double ring. The outer lens is manifested as a weak exponential sub-section at $r = 20''-35''$. In our decomposition the two lenses were fitted by Ferrers functions. For this galaxy the typically used Ferrers index $n = 1$ gave too sharp outer edges for the lenses. Therefore, the Ferrers index was left free for fitting, leading to $n = 2.6$ and 6 for the inner and outer lenses, respectively. Our solution did not converge, but at the end it changed very slowly.

NGC 7371: This galaxy has a weak bar, whereas outside the bar flocculent spiral arms dominate the disk. It is due to the spiral arms that the exponential function is not a perfect fit to the outer disk. Using a Ferrers function for the bar in the decomposition gave a good fit to the observed image. Notice the extremely small B/T flux-ratio of 0.10 for this galaxy.

NGC 7377: This galaxy has flocculent spiral arms in the optical region, but in our near-IR image the spirals arms are absent. The galaxy has a bright lens, manifested as an exponential sub-section in the surface brightness profile. In the decomposition a Ferrers function was used for the lens which considerably improved the model. After subtracting the bulge model from the original image a weak bar was visible in the residual image (see SLBK).

NGC 7585: NGC 7585 is classified as a peculiar S0 galaxy in RC3. Indeed, the peculiar disk is dominating this galaxy. The galaxy has also a lens with slightly boxy isophotes. The lens is visible in the direct image and manifested also in the surface brightness profile. In the decomposition the lens was fitted by a Ferrers function. The residual image, after subtracting the bulge model, shows a nuclear disk with spiral arms at $r < 4''$ (see SLBK).

NGC 7727: : The galaxy has a small classical bar and a perturbed peculiar disk. The dominant feature in the disk is a lens-like component with some spiral structure. In the decomposition the bar was fitted by a Ferrers function. We added to the decomposition also another Ferrers function, representing the flux in the complicated structural components outside the bar, but it did not affect the parameters of the bulge or the disk.

NGC 7742: This galaxy is classified Sb in RC3, but in the K_s -band image it has no spiral structure. The galaxy has two lenses: an inner lens at $r < 10''$, characterized also by a double ring, and an outer lens, manifested as a bump at $r = 15-25''$ in the surface brightness profile. In our decomposition we first tried to fit both lenses with Ferrers functions, but after a few iterations the inner lens disappeared.

NGC 7796: This galaxy is classified as an elliptical galaxy both in RC3 and in CAG. However, our K_s -band surface brightness profile shows that the galaxy has a disk, which is exponential at a large radial range. Also, it was not possible to fit the surface brightness profile by a single de Vaucouleurs type Sérsic function, thus confirming that the galaxy is an S0. A good solution was found by fitting a bulge and a disk.

Table 1. Parameters of the bulge and the disk, derived from 2D-decompositions. All parameters are uncorrected for the effects of dust, except for B/T (corr) in which both Galactic and internal dust effects are corrected.

Galaxy	inc [deg]	n	r_{eff} [kpc]	$M_K(bulge)$	h_r [kpc]	μ_o^{obs} [mag arcsec ⁻²]	B/T	B/T (corr)
ESO 137-G10	45.0	1.4	1.14	-23.24	4.15	16.90	0.25	0.26
ESO 208-G21 ^d	43.8	4.2	0.62	-22.60	0.08 ^c	13.81 ^c	0.97	0.97
ESO 337-G10	37.6	1.7	1.52	-24.33	6.03	17.52	0.41	0.43
IC 1392	47.2	1.6	0.79	-23.80	3.94	16.65	0.28	0.30
IC 4214	47.6	2.9	0.60	-22.97	4.96	18.16	0.28	0.30
IC 4329	56.0	1.5	0.88	-23.71	9.97	17.20	0.13	0.14
IC 4889	42.3	2.3	0.99	-23.52	3.06	16.71	0.37	0.39
IC 4991	44.6	1.6	2.83	-24.90	9.94	17.65	0.36	0.38
IC 5267	33.7	2.2	0.82	-22.84	6.26	18.22	0.20	0.21
IC 5328	49.9	2.7	1.37	-23.80	5.34	17.51	0.37	0.40
NGC 439 ^d	49.2	3.7	17.9	-26.20				
NGC 474	23.6	1.8	0.57	-22.70	4.01	17.66	0.25	0.27
NGC 484	45.1	2.8	1.69	-24.63	5.89	17.94	0.62	0.64
NGC 507	27.6	2.7	2.36	-24.81	9.48	17.65	0.31	0.33
NGC 524	17.4	2.7	1.39	-24.10	4.12	16.62	0.28	0.29
NGC 584	51.3	2.6	1.27	-23.93	4.37	17.75	0.58	0.61
NGC 718 ^a	31.6	1.7	0.22	-21.37	2.30	17.58	0.21	0.22
NGC 890	46.1	3.2	2.53	-24.55	4.91	16.80	0.42	0.44
NGC 936 ^a	42.3	1.5	0.29	-21.90	3.06	16.80	0.12	0.13
NGC 1022 ^a	21.6	2.2	0.13	-20.48	1.80	17.12	0.10	0.11
NGC 1079 ^b	53.9	2.2	0.42	-21.34	2.81	18.42	0.25	0.28
NGC 1161	33.6	2.5	1.77	-24.20	4.45	18.19	0.65	0.67
NGC 1201	53.1	3.4	0.82	-22.82	2.85	16.98	0.37	0.40
NGC 1302	15.1	2.2	0.48	-22.24	3.34	17.77	0.24	0.26
NGC 1317 ^b	17.6	2.1	0.46	-22.21	2.12	17.44	0.34	0.35
NGC 1326 ^b	38.7	3.0	0.57	-22.55	3.00	17.64	0.34	0.36
NGC 1344	44.7	3.1	1.28	-22.88	3.71	18.37	0.52	0.54
NGC 1350 ^b	54.2	2.2	0.68	-22.56	11.5	19.58	0.25	0.27
NGC 1351	55.1	3.3	0.77	-22.02	3.02	18.47	0.53	0.56
NGC 1371	43.7	1.4	0.26	-20.83	2.55	16.83	0.08	0.08
NGC 1380	42.3	2.1	0.97	-23.19	2.87	16.56	0.31	0.33
NGC 1387 ^b	3.5	1.8	0.38	-22.80	2.40	17.30	0.39	0.41
NGC 1389	58.8	1.7	0.40	-21.53	1.81	17.22	0.36	0.39
NGC 1400 ^a	23.8	2.5	0.15	-19.98	0.46	16.83	0.50	0.52
NGC 1411 ^b	40.6	2.0	0.04	-19.36	0.98	16.60	0.08	0.08
NGC 1415 ^a	67.0	1.3	0.16	-20.60			0.11	0.13
NGC 1440 ^a	39.0	1.4	0.21	-21.06	1.82	16.86	0.14	0.15
NGC 1452 ^a	45.7	1.6	0.44	-21.76	3.37	18.01	0.22	0.24
NGC 1512 ^b	52.8	1.2	0.27	-20.49	1.69	17.04	0.19	0.20
NGC 1533 ^b	19.6	1.5	0.25	-21.53	1.63	17.20	0.25	0.26
NGC 1537	51.9	2.9	0.61	-22.62	2.10	17.19	0.52	0.55
NGC 1543	0.0	2.5	0.99	-22.68	9.94	19.71	0.32	0.34
NGC 1553	41.5	2.1	0.63	-22.85	3.23	16.87	0.21	0.23
NGC 1574 ^b	16.8	2.8	0.42	-22.52	2.22	17.33	0.38	0.40
NGC 1617	61.2	1.6	0.27	-21.46	2.06	16.14	0.15	0.17
NGC 2196 ^a	45.8	2.8	1.55	-23.12	3.78	17.14	0.30	0.32
NGC 2217	29.5	2.6	0.89	-23.24	10.1	18.59	0.33	0.34
NGC 2273 ^a	53.6	1.8	0.36	-22.18	3.49	17.49	0.24	0.26
NGC 2300	41.4	1.3	0.87	-23.53	3.92	16.64	0.26	0.28
NGC 2460 ^b	41.4	2.6	0.71	-21.91	1.22	15.76	0.27	0.29
NGC 2655	36.9	3.8	2.40	-24.42	3.59	17.38	0.66	0.68
NGC 2681 ^a	24.2	2.2	0.12	-21.72	2.18	17.45	0.24	0.25
NGC 2685	50.3	2.8	0.26	-21.29	1.85	17.53	0.27	0.29
NGC 2768	66.4	2.5	1.28	-23.38	4.89	16.78	0.30	0.35
NGC 2781 ^a	59.1	2.9	0.77	-22.60	7.39	19.23	0.30	0.33
NGC 2782	34.2	3.2	0.57	-22.66	3.45	17.31	0.25	0.26
NGC 2787	55.6	1.3	0.21	-21.51	1.49	15.95	0.18	0.20
NGC 2855 ^a	33.1	2.8	2.10	-23.68	4.16	18.04	0.57	0.59
NGC 2859 ^a	40.5	1.3	0.63	-22.99	9.76	19.35	0.28	0.29
NGC 2880	52.0	2.3	0.70	-22.58	3.07	17.62	0.42	0.45
NGC 2902	23.9	2.0	0.31	-22.05	1.89	17.25	0.32	0.33

...continue

Galaxy	inc [deg]	n	r_{eff} [kpc]	$M_K(bulge)$	h_r [kpc]	μ_o^{obs} [mag arcsec ⁻²]	B/T	B/T (corr)
NGC 2911 ^a	40.4	3.1	1.44	-23.70	8.57	18.36	0.34	0.35
NGC 2950	53.2	2.4	0.49	-23.07	3.62	17.77	0.42	0.45
NGC 2983 ^a	54.9	1.3	0.29	-21.45	3.71	17.42	0.11	0.12
NGC 3032	29.9	2.4	0.10	-20.70	1.51	17.27	0.19	0.20
NGC 3081 ^b	30.6	2.1	0.24	-21.29	3.30	17.93	0.10	0.11
NGC 3100 ^b	52.9	1.8	0.96	-22.52	4.95	18.06	0.30	0.32
NGC 3166	60.7	0.8	0.43	-22.85			0.23	0.26
NGC 3169	51.9	2.9	0.94	-23.62	3.16	17.22	0.58	0.60
NGC 3245	51.6	2.4	0.40	-22.69	2.29	16.49	0.33	0.36
NGC 3358 ^b	54.5	1.7	0.48	-22.57	10.8	18.26	0.11	0.12
NGC 3384	59.7	1.5	0.21	-21.50	1.37	16.22	0.32	0.35
NGC 3414 ^a	31.1	2.6	0.54	-22.95	3.02	17.07	0.32	0.33
NGC 3489	49.7	2.1	0.07	-20.00	0.52	15.54	0.23	0.24
NGC 3516	38.7	3.4	0.26	-23.54	4.90	18.11	0.40	0.42
NGC 3607	23.3	1.5	0.63	-23.22	1.99	15.98	0.32	0.33
NGC 3626 ^a	45.9	1.9	0.34	-22.58	3.18	17.11	0.25	0.27
NGC 3665	39.1	2.7	1.98	-24.36	4.61	17.55	0.58	0.60
NGC 3706 ^{b,d}	50.7	3.5	6.79	-25.23			0.92	0.93
NGC 3729	49.6	1.3	0.15	-18.97	1.71	16.61	0.03	0.04
NGC 3892	13.1	2.9	0.40	-21.63	3.46	17.44	0.10	0.11
NGC 3941 ^a	44.4	1.6	0.22	-22.17	2.03	16.07	0.17	0.18
NGC 3945 ^a	47.9	2.9	0.77	-23.15	12.7	19.96	0.37	0.39
NGC 3998	38.0	2.0	0.40	-23.23			0.36	0.38
NGC 4138	52.4	1.7	0.08	-20.18	1.08	15.36	0.08	0.08
NGC 4143	49.6	1.1	0.23	-21.88	1.01	15.21	0.27	0.29
NGC 4150	47.5	2.8	0.14	-20.11	0.65	16.59	0.38	0.40
NGC 4203	28.7	2.7	0.27	-21.46	1.55	17.31	0.36	0.38
NGC 4245	34.6	1.7	0.22	-20.11	1.22	17.52	0.22	0.24
NGC 4262	28.8	1.6	0.25	-22.07	1.13	16.86	0.54	0.55
NGC 4267	18.6	1.5	0.28	-22.04	2.06	17.18	0.30	0.31
NGC 4314	27.1	1.5	0.22	-20.40	1.52	17.34	0.16	0.17
NGC 4340 ^a	56.2	3.4	0.78	-21.91	3.62	17.65	0.26	0.29
NGC 4369	13.4			-21.80	1.54	17.11	0.34	0.36
NGC 4371	59.2	2.6	0.53	-21.78	2.54	16.75	0.20	0.22
NGC 4373	0.0	2.7	2.40	-24.95	10.1	18.66	0.53	0.54
NGC 4378	37.2	2.4	0.83	-23.17	4.90	18.05	0.32	0.34
NGC 4424	68.4			-19.70	2.39	17.37	0.10	0.12
NGC 4435	45.4	1.3	0.30	-22.08	1.64	16.49	0.28	0.30
NGC 4457	24.4	1.5	0.22	-22.07			0.28	0.29
NGC 4459	45.6	3.0	0.49	-22.76	2.04	16.41	0.35	0.37
NGC 4477	34.2	2.5	0.34	-21.93	2.04	16.41	0.17	0.18
NGC 4546	58.0	1.8	0.32	-22.85	2.02	15.79	0.29	0.32
NGC 4596 ^a	44.3	1.6	0.29	-21.67	3.32	17.34	0.13	0.14
NGC 4608 ^a	31.1	1.4	0.27	-21.14	3.03	18.06	0.14	0.15
NGC 4612	46.4	2.2	0.24	-20.98			0.21	0.22
NGC 4643	38.5	0.8	0.39	-22.68	3.86	17.06	0.15	0.15
NGC 4694	58.9	1.9	1.16	-22.88	2.15	17.98	0.65	0.68
NGC 4696	43.9	1.4	1.56	-23.81	8.42	16.78	0.11	0.12
NGC 4754	60.1	1.9	0.24	-21.81	2.65	16.79	0.18	0.20
NGC 4772	60.8	2.8	0.61	-21.86			0.39	0.43
NGC 4880	41.4	3.2	0.24	-17.51	1.63	17.64	0.02	0.02
NGC 4976	55.6	2.0	0.24	-22.45	2.91	15.84	0.12	0.14
NGC 4984	55.8	2.3	0.59	-22.99	2.41	16.64	0.41	0.44
NGC 5026	55.7	2.7	1.28	-23.68	6.46	17.06	0.21	0.23
NGC 5087 ^d	21.9	4.1	1.40	-24.58				
NGC 5121	37.0	2.2	0.24	-21.92	1.85	17.06	0.28	0.29
NGC 5206	24.6	3.0	0.18	-17.40	1.10	18.16	0.09	0.20
NGC 5266	54.2	2.8	1.84	-24.79	7.94	17.44	0.45	0.48
NGC 5273	30.8	1.6	0.19	-20.63	1.90	16.90	0.11	0.11

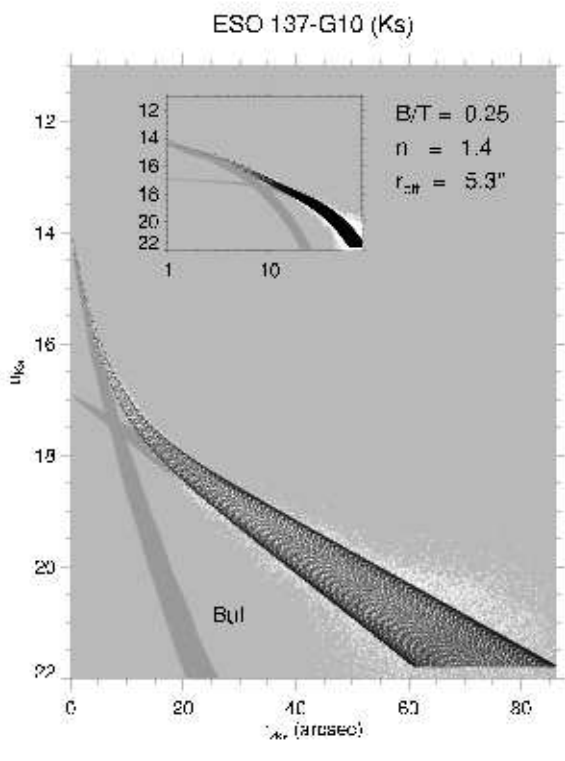
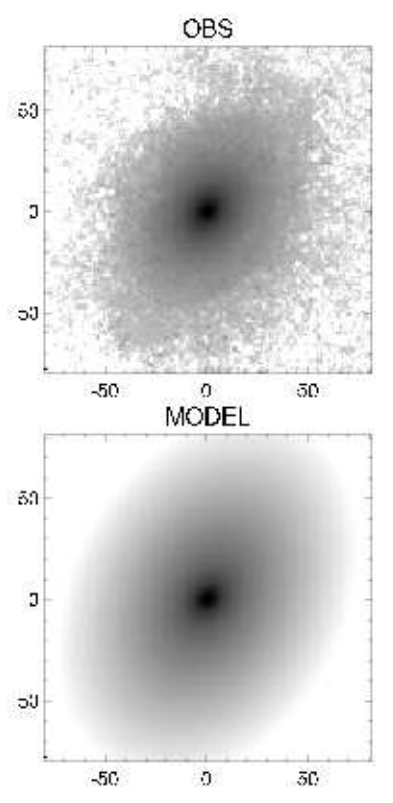
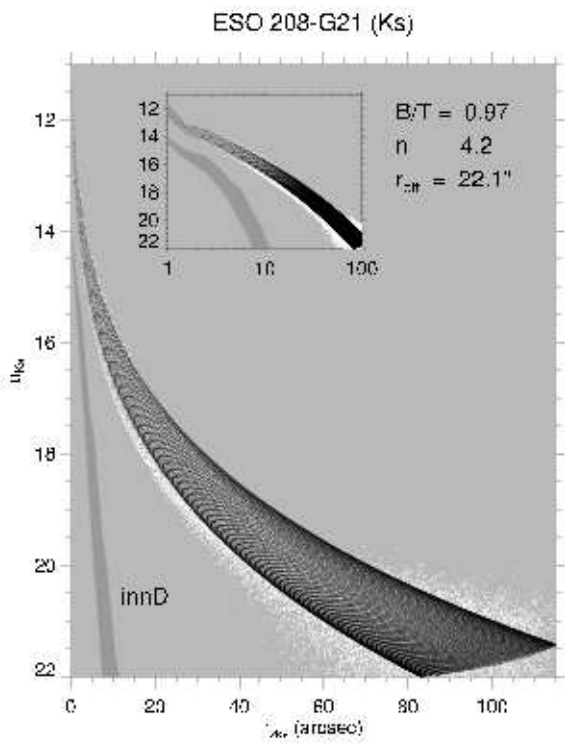
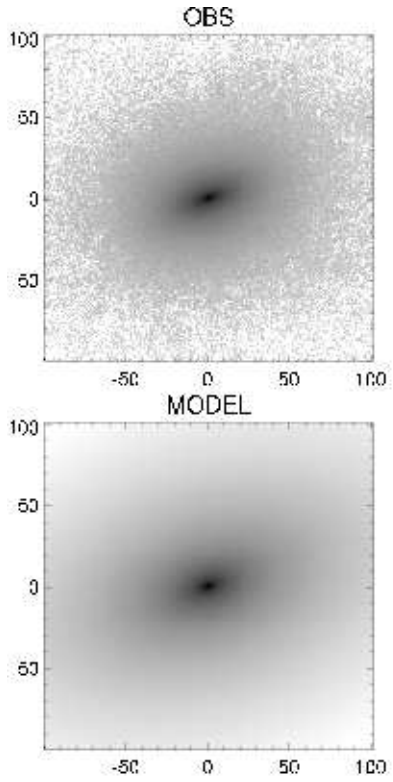
continue

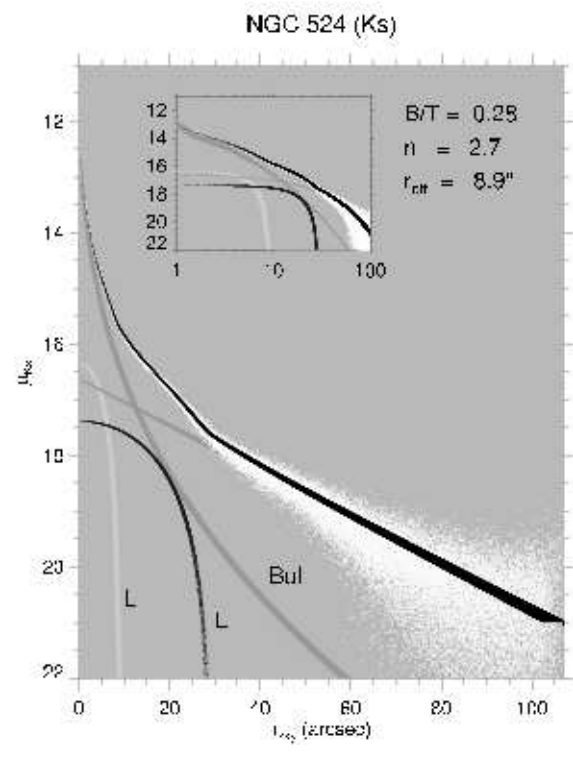
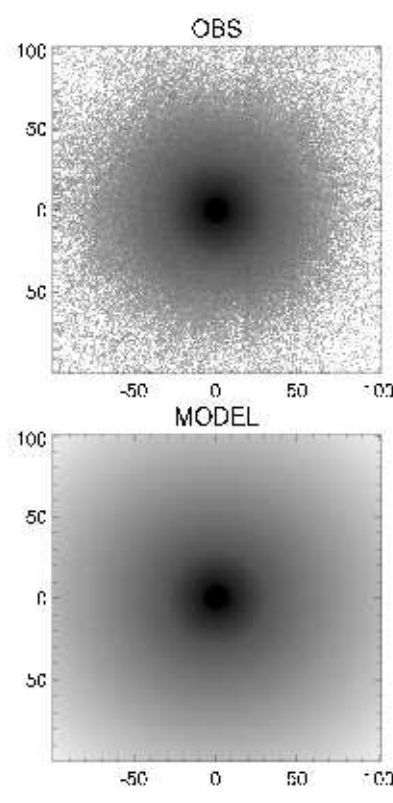
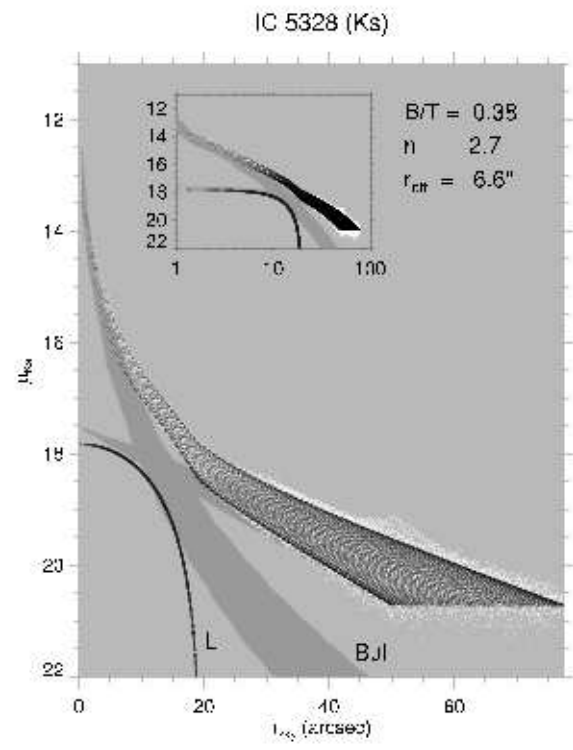
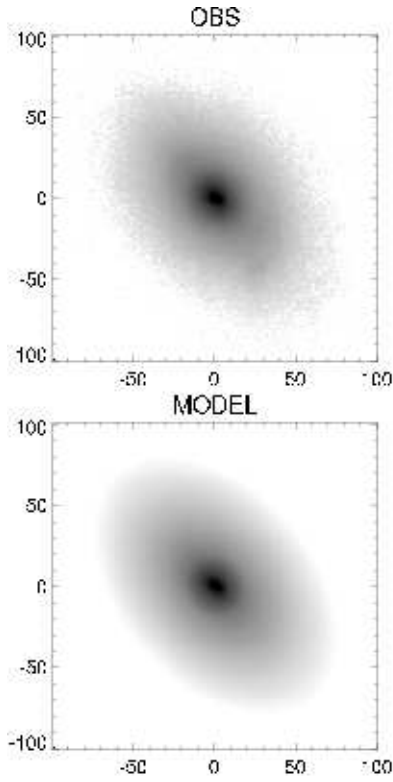
Galaxy	inc [deg]	n	r_{eff} [kpc]	$M_K(bulge)$	h_r [kpc]	μ_o^{obs} [mag arcsec ⁻²]	B/T	B/T (corr)
NGC 5333	59.3	3.8	0.59	-23.67	3.23	16.92	0.47	0.51
NGC 5365	52.1	2.0	0.52	-23.08	9.38	18.48	0.17	0.19
NGC 5377	57.4	1.9	0.52	-22.35	2.94	16.69	0.19	0.21
NGC 5419	43.9	1.4	1.74	-24.60	8.57	17.09	0.24	0.25
NGC 5473	36.2	1.9	0.40	-22.77	2.61	16.62	0.26	0.27
NGC 5485	46.4	2.3	1.66	-23.51	4.47	17.89	0.48	0.51
NGC 5493	29.8	2.1	1.02	-23.77	2.40	16.76	0.50	0.52
NGC 5631	20.8	3.2	0.90	-23.30			0.45	0.46
NGC 5636	25.2	2.1	0.90	-23.06	2.59	17.11	0.41	0.42
NGC 5728	41.3	0.6	0.69	-23.08	10.05	18.81	0.17	0.18
NGC 5750	61.0	4.2	1.11	-22.80	3.31	16.73	0.31	0.34
NGC 5846	24.0	1.7	2.34	-24.41	4.74	17.32	0.46	0.47
NGC 5898	28.8	2.2	0.92	-23.78	4.17	17.57	0.43	0.45
NGC 5953	33.7	2.7	0.24	-21.99	1.36	16.32	0.26	0.28
NGC 5982	36.5	2.7 ^d	0.30	-20.14	1.67 ^c	18.58 ^c	0.26	0.28
NGC 6340	15.0	2.6	0.45	-21.91	2.62	17.17	0.19	0.20
NGC 6407	35.7	1.5	1.21	-23.66	5.69	17.04	0.20	0.21
NGC 6646	23.4	2.2	2.16	-24.16	7.76	17.59	0.25	0.26
NGC 6654	38.1	1.5	0.33	-21.93	4.96	17.68	0.11	0.12
NGC 6684	49.2	3.4	0.63	-21.98	2.15	17.26	0.36	0.39
NGC 6703	14.1	2.5	0.73	-23.47	3.58	17.13	0.30	0.32
NGC 6782	22.3	2.1	0.60	-22.95	4.62	18.11	0.20	0.21
NGC 6861	43.0	2.0	0.96	-24.09	5.22	17.54	0.36	0.38
NGC 6958	35.7	3.3	0.96	-23.85	7.89	18.72	0.43	0.45
NGC 7029	53.0	1.8	0.80	-23.24			0.37	0.40
NGC 7049	39.1	2.7	2.42	-24.81	6.15	18.81	0.79	0.81
NGC 7079	46.0	1.4	0.39	-22.34	2.11	16.08	0.21	0.23
NGC 7098	55.1	2.2	0.63	-22.83	4.99	17.56	0.25	0.27
NGC 7192	15.9	2.7	1.38	-23.68	5.85	18.71	0.44	0.45
NGC 7213	0.0	2.9	0.33	-22.76	2.61	16.56	0.17	0.18
NGC 7371	20.7	2.1	0.49	-21.05	2.81	17.40	0.10	0.11
NGC 7377	37.3	2.5	2.19	-23.98	8.21	17.79	0.26	0.28
NGC 7457	57.1	3.1	0.48	-20.48	1.54	16.83	0.20	0.22
NGC 7585	36.3	2.4	1.47	-24.00	6.17	17.47	0.29	0.31
NGC 7727	43.1	3.2	0.94	-23.16	3.22	17.23	0.38	0.40
NGC 7742	10.6	3.9	0.23	-21.42	1.15	16.20	0.22	0.23
NGC 7743	40.3	2.5	0.20	-21.48	3.24	17.20	0.11	0.12
NGC 7796	27.9	2.2	1.56	-24.26	5.69	17.84	0.48	0.49

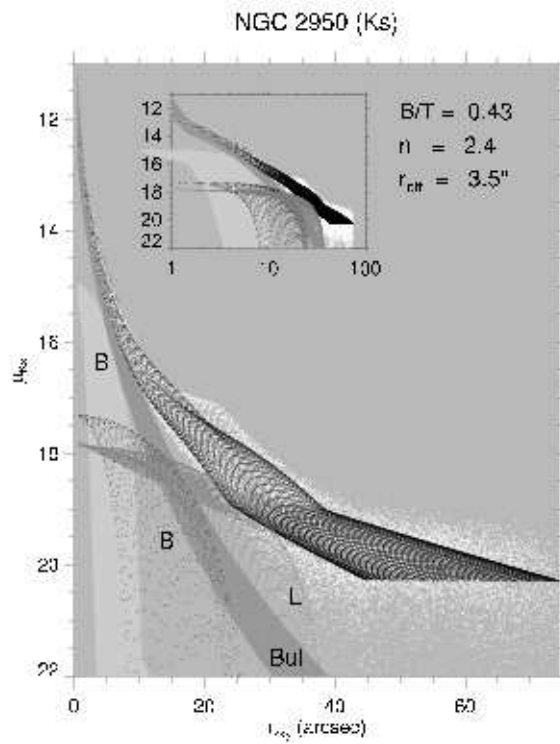
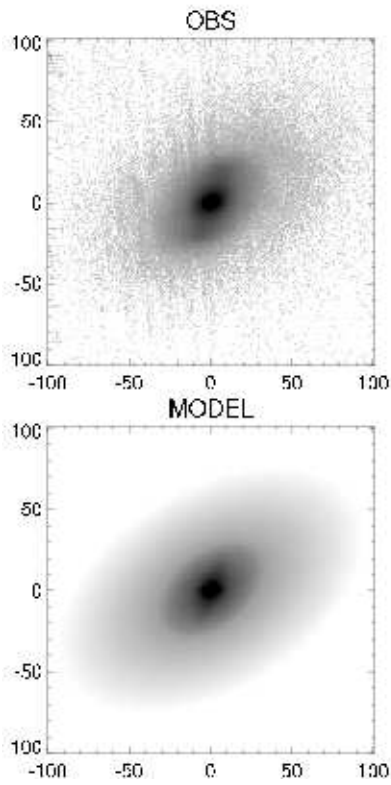
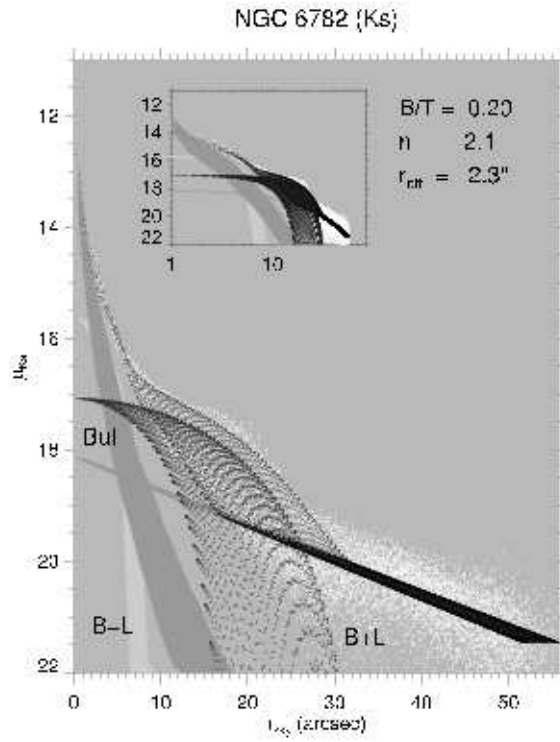
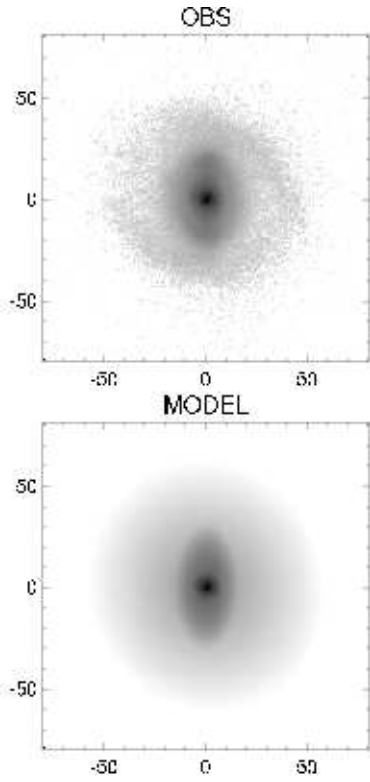
^a from Laurikainen et al. 2005^b from Laurikainen et al. 2006^c inner disk^d elliptical galaxy

Table 2. Mean total absolute magnitudes and the parameters of the bulge (median and mean) in different Hubble type bins. Except for n and r_{eff} , the values are corrected for Galactic and internal extinction. The uncertainties are standard deviations in the bins.

Type	N	$\langle M_{tot}^o \rangle$	$\langle B/T \rangle$ (corr) mean (median)	$\langle n \rangle$ mean (median)	$\langle r_{eff}/h_r^o \rangle$ mean (median)
NIRSOS:					
-3	35	-24.44	0.39±0.13 (0.39)	2.230±0.62 (2.18)	0.24±0.100 (0.23)
-2	35	-24.00	0.33±0.14 (0.33)	2.265±0.72 (2.38)	0.19±0.103 (0.18)
-1	26	-23.82	0.29±0.13 (0.29)	2.227±0.59 (2.13)	0.19±0.108 (0.19)
0	21	-24.13	0.27±0.15 (0.23)	2.074±0.74 (2.11)	0.20±0.139 (0.14)
1	26	-23.53	0.25±0.12 (0.26)	2.146±0.64 (2.22)	0.18±0.122 (0.15)
OSUBSGS:					
2	17	-23.91	0.25±0.13 (0.23)	1.69±0.60 (1.48)	0.15±0.15 (0.09)
3	20	-23.85	0.14±0.09 (0.12)	1.49±0.83 (1.29)	0.12±0.07 (0.09)
4	38	-23.89	0.11±0.08 (0.09)	1.44±0.77 (1.27)	0.15±0.13 (0.11)
5	30	-23.22	0.11±0.13 (0.06)	1.42±0.70 (1.31)	0.16±0.16 (0.08)
6	13	-22.03	0.05±0.10 (0.01)	1.45±1.15 (1.14)	0.16±0.24 (0.06)
7	6	-22.55	0.09±0.13 (0.06)	1.53±0.95 (2.06)	0.46±0.39 (0.39)
8	2	-22.63	0.05±0.06 (0.09)	1.15±1.23 (2.02)	0.12±0.10 (0.19)
9	3	-21.00	0.04±0.05 (0.00)	2.01±0.22 (2.07)	0.30±0.43 (0.06)







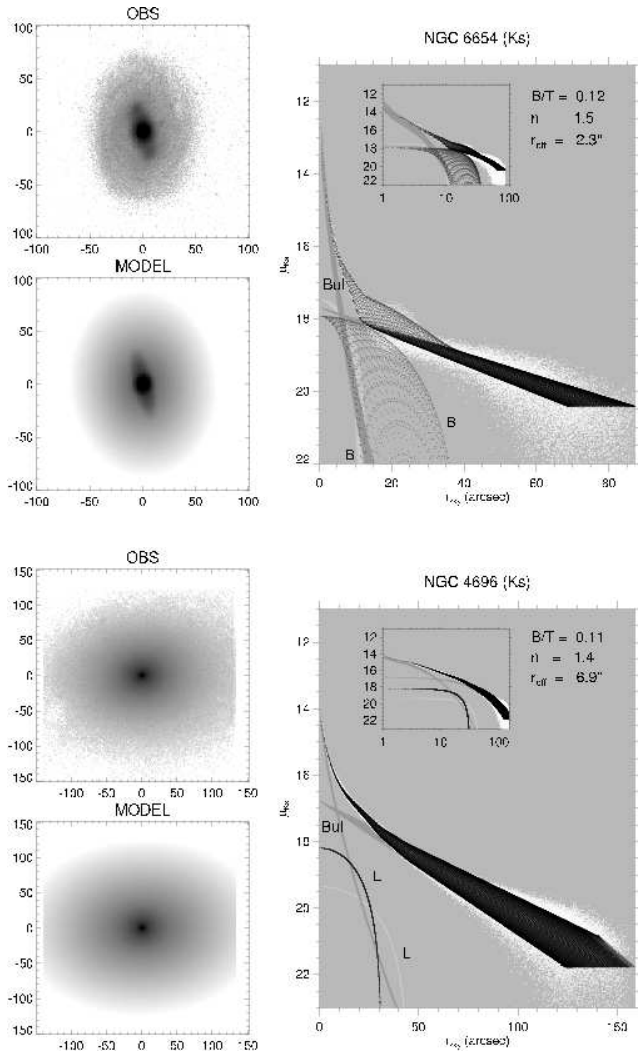


Figure 1. Multi-component structural decompositions for 160 of the 175 galaxies of our sample. In the figure representative examples for 8 galaxies are shown (the rest of them are available in electronic form). *Right panel* shows the decomposition, whereas the two left panels show the observed image (above) and the model image (below). White dots in the right panel show the data points of the 2-dimensional surface brightness distribution (brightness of each pixel as a function of sky-plane radius from the galaxy center), and the black and grey colors show the model components. The uppermost black dots show the total model. In the figures a bulge is indicated by “Bul”, a lens by “L”, a bar by “B”. In some cases a bar and lens are fitted by a single function in which case the designation is “B+L”. The small inserts show the same decompositions in a logarithmic radial scale.

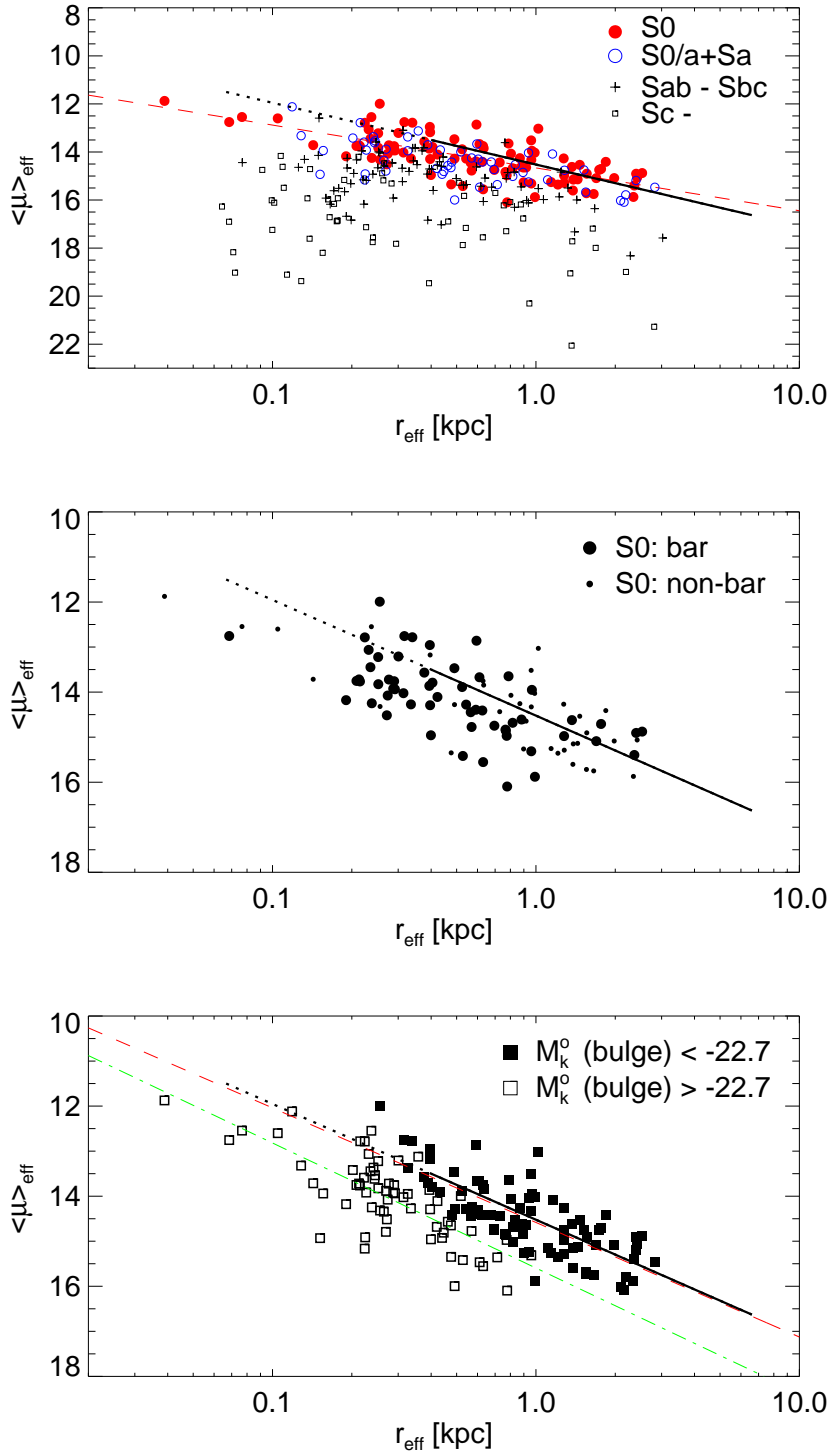


Figure 2. The Kormendy relation, which is an empirical relation between the effective radius of the bulge, r_{eff} , and the mean surface brightness of the bulge inside r_{eff} , denoted by $\langle \mu \rangle_{\text{eff}}$. *The top panel* shows the relation separately for S0s (filled red circles), S0/a+Sa spirals (open blue circles), Sab-Sbc spirals (crosses) and Sc and later-type spirals (squares). *The middle panel* shows the barred (large filled circles) and non-barred (small dots) S0s, whereas *The lower panel* shows separately the bright (filled symbols) and dim (open symbols) bulges (S0-Sa) in NIRS0S. The solid line in all panels indicates the location of the Coma cluster ellipticals, taken from Khosroshahi et al. (2000): $\langle \mu \rangle_{\text{eff}} = 2.57 \log r_{\text{eff}} + 14.07$. The dotted section of the line is an extrapolation of the Coma cluster ellipticals to smaller r_{eff} . The difference in H_0 between Khosroshahi et al. ($H_0=50 \text{ km sec}^{-2} \text{ Mpc}^{-1}$) and this work ($H_0=75 \text{ km sec}^{-2} \text{ Mpc}^{-1}$) has been taken into account in this figure and in Fig. 3. In the upper panel the red dashed line is a fit to the S0 data points. In the lower panel the red dashed and green dash-dotted lines are linear fits for the bright and dim bulges, respectively. Note the different scale in the uppermost frame. The same symbols are consistently used in the subsequent type.

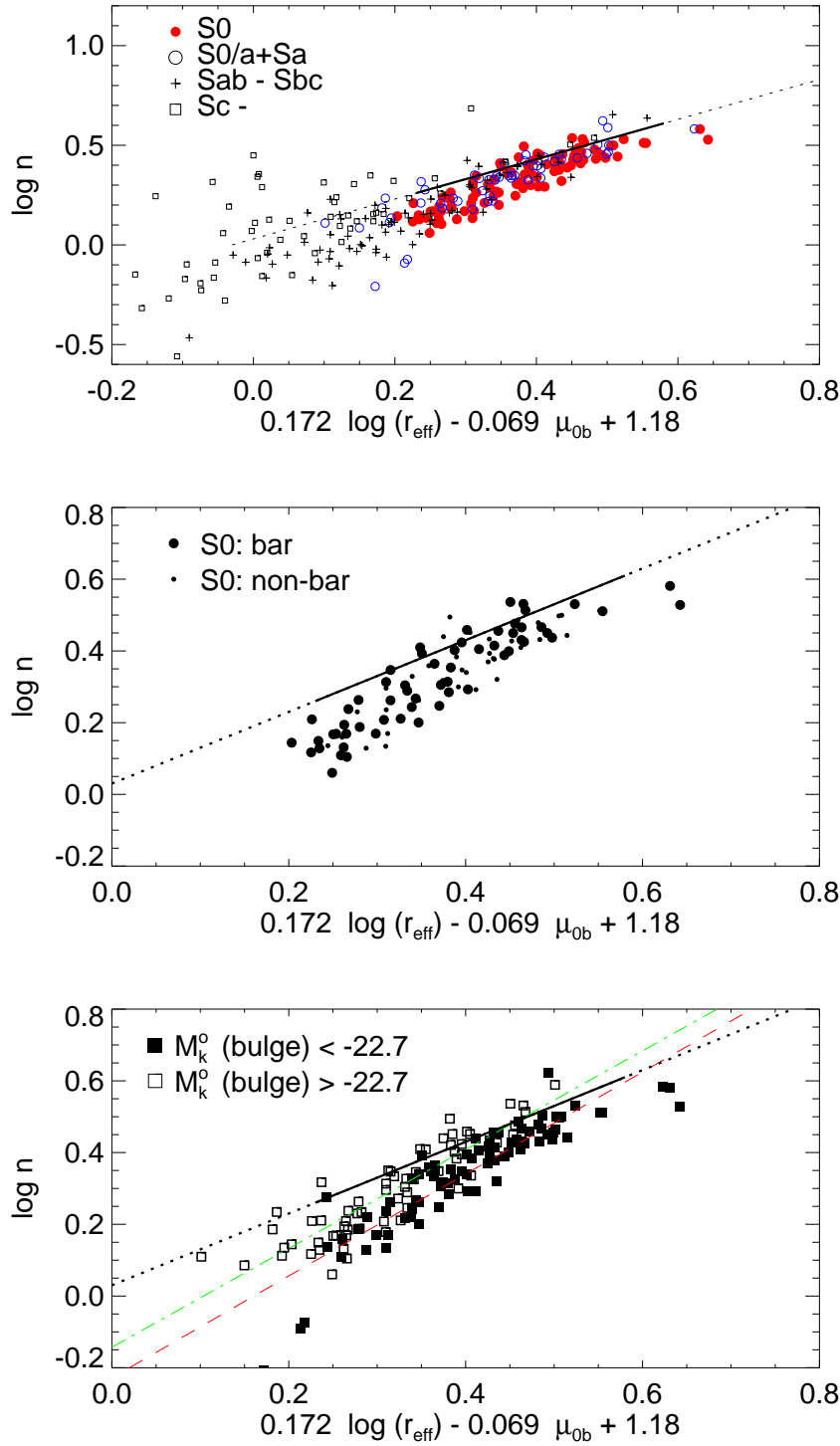


Figure 3. Projections of the photometric plane, which is a relation between three parameters of the bulge, the Sérsic index n , the effective radius r_{eff} in [kpc], and the central surface brightness μ_{ob} of the bulge. The full line indicates the best-fit plane for the Coma cluster ellipticals, taken from Khosroshahi et al. (2000). The Coma cluster ellipticals does not go through the origin because of the correction made to Hubble constant. The dotted line shows an extrapolation outside the Coma cluster ellipticals. The symbols are the same as in Fig. 2. In the lower panel the red dashed and green dash-dotted lines indicate the best fits for the bright and the dim bulges in NIRS0S, respectively.

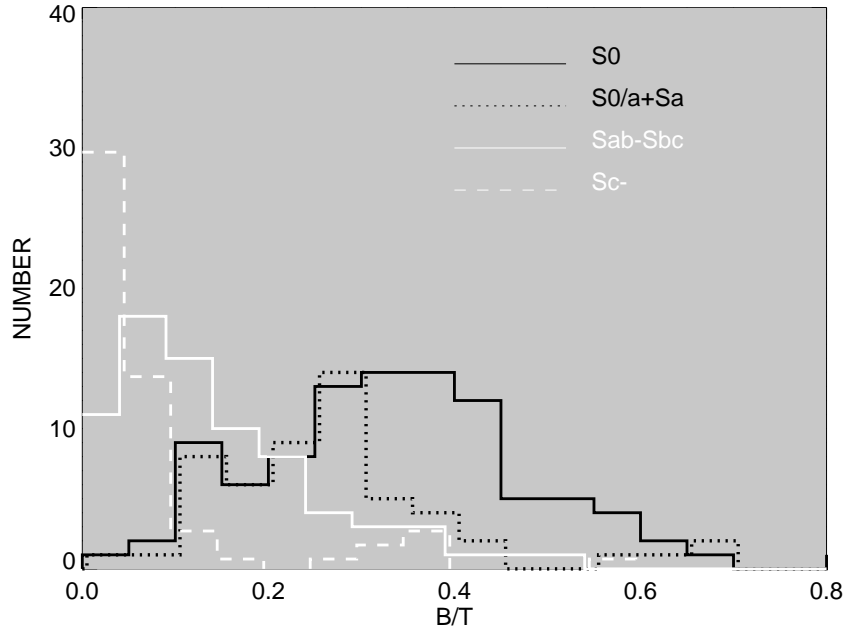


Figure 4. Histograms of the B/T flux ratios, corrected for Galactic and internal dust, as explained in Section 4. The histograms are shown for the S0s in NIRS0S (full black line), S0/a+Sa galaxies in NIRS0S (dotted black line), Sab-Sbc galaxies in OSUBSGS (white full line), and Sc and later types in OSUBSGS (white dashed line). The decompositions for the OSUBSGS galaxies are made using H -band images, and for the NIRS0S galaxies using K_s -band images. However, using the overlapping Sa-galaxies we checked that there is no offset between the two samples.

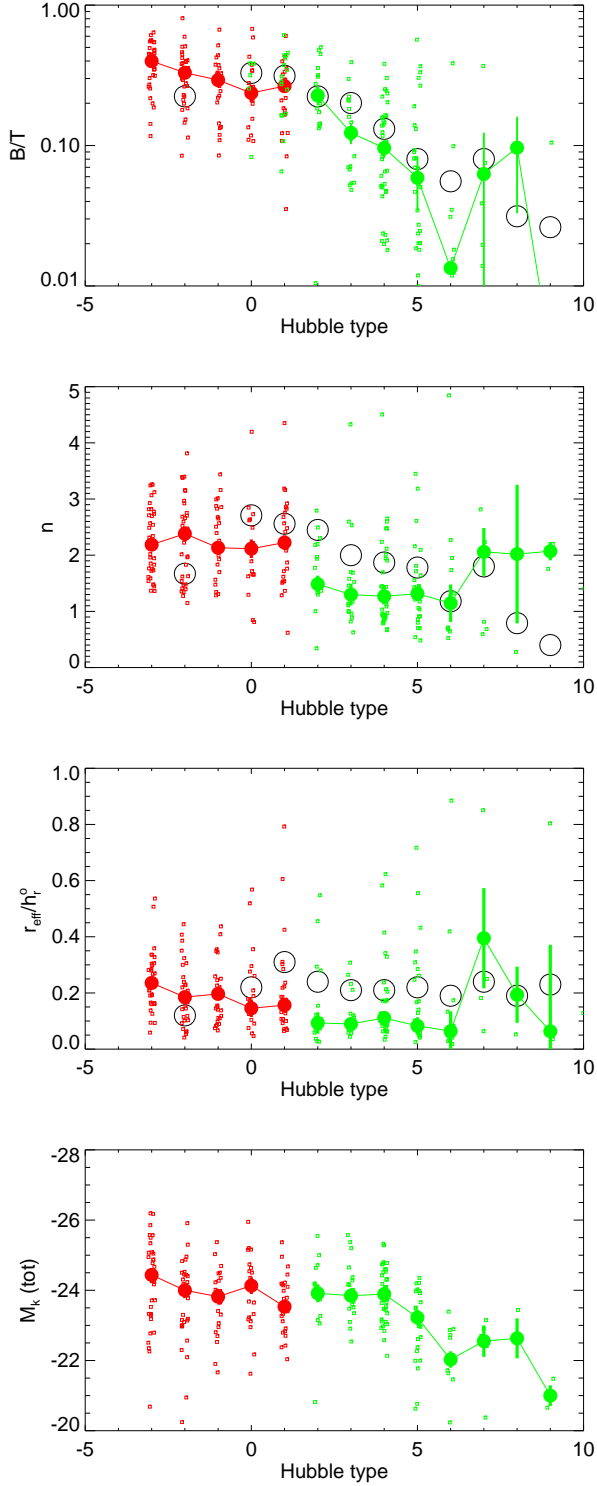


Figure 5. As a function of Hubble type are shown: (a) the dust bulge-to-total flux ratio (B/T) corrected for Galactic and internal dust, (b) Sérsic index n , (c) the ratio of the effective radius of the bulge (r_{eff}) divided by the scale length of the disk (h_r^0), and (d) the total absolute galaxy magnitude corrected for Galactic extinction (M_{tot}^0). The *small symbols* show the measurements for the individual galaxies (with a small random horizontal offset), *filled circles* show the median values in each Hubble type bin, and *large open circles* are the median values from Graham & Worley (2008; their value for S0s refers to types -3, -2, -1, and is here drawn at $T=-2$). The error bars are taken to be the standard errors of the mean (= sample variance in each bin divided by square root of the number of galaxies in each bin), which stresses the large number of galaxies in the bin. Red colour is for the galaxies in NIRS0S and green for those in OSUBSGS.

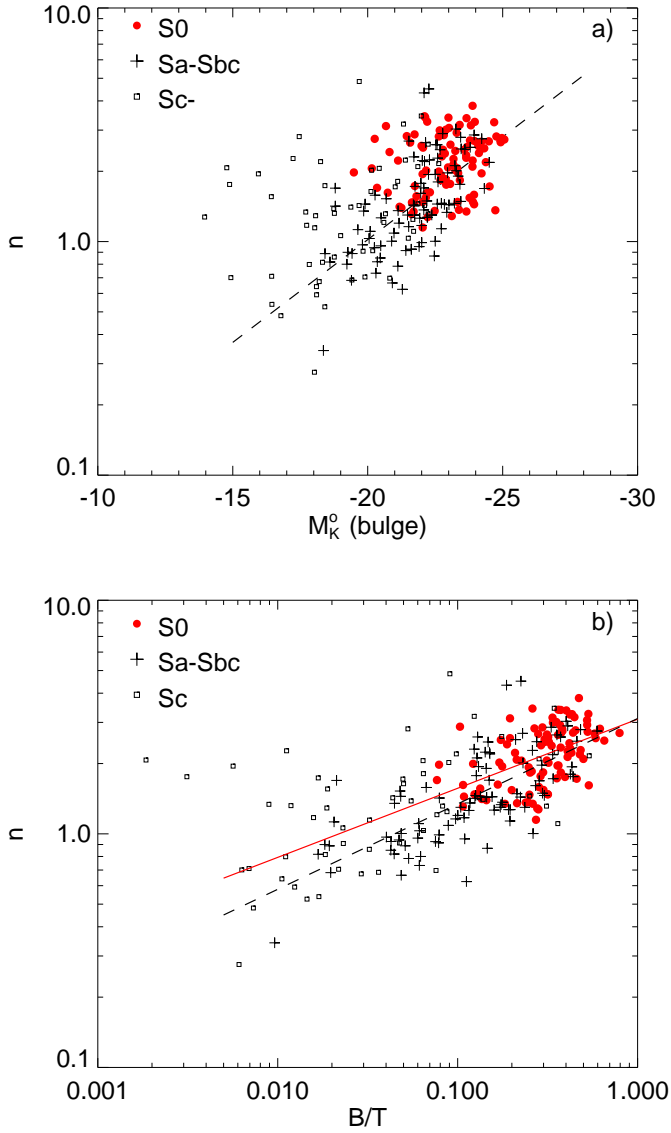


Figure 6. a) The Sérsic index n is plotted against the absolute brightness of the bulge corrected for Galactic and internal extinction ($M_K(\text{bulge})$): S0s (red filled circles) are from NIRS0S, whereas Sa-Sbc (crosses) and Sc and later types (squares) are from OSUBSGS. Dashed line indicates the linear fit for Sa-Sbc galaxies; for S0s there is no statistically significant correlation (significance level of rank correlation coefficient is 0.03) b) Dust corrected bulge-to-total flux ratio (B/T) is correlated with the Sérsic index. The continuous and dashed lines are the linear fits for S0s and for Sa-Sbc galaxies, respectively. Both correlations are statistically significant. S0/a galaxies from NIRS0S fall largely on top of S0s, and for clarity are not shown.

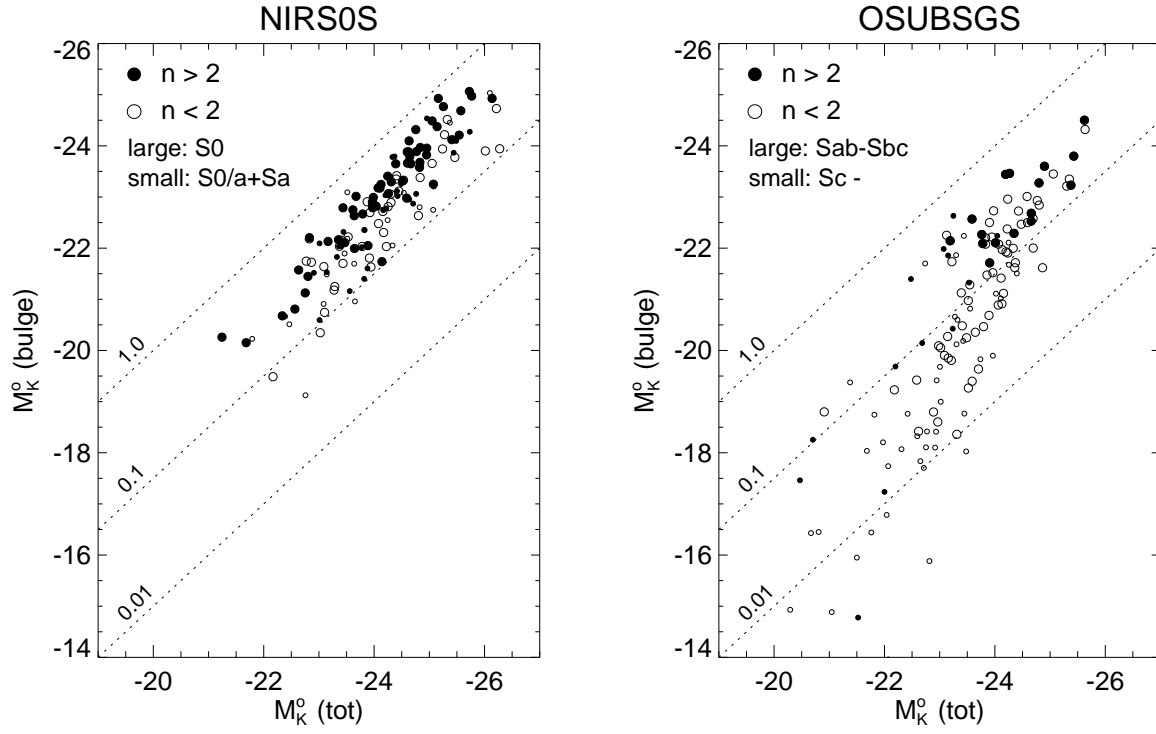


Figure 7. The absolute brightness of the bulge ($M_K^o(\text{bulge})$) is shown as a function of the total absolute galaxy brightness ($M_K^o(\text{tot})$), both being corrected for Galactic and internal dust. The dashed lines denote $B/T = 0.01, 0.1$ and 1.0 . *Left panel:* S0s (large symbols) and S0/a-Sa galaxies (small symbols) in NIRS0S, both divided in two Sérsic index bins (filled symbols for $n > 2$, open symbols for $n < 2$). *Right panel:* Sa-Sbc (large symbols) and Sc and later types (small symbols), again in two Sérsic index bins.

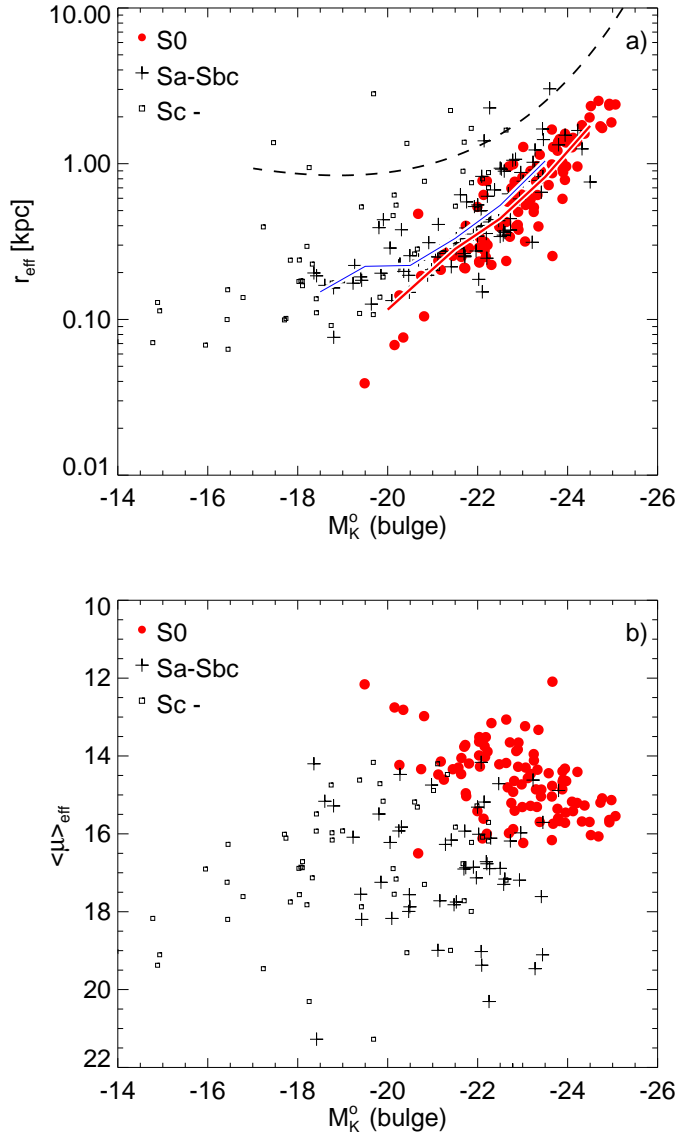


Figure 8. (a) The effective radius of the bulge (r_{eff}) plotted against the absolute brightness of the bulge ($M_K^o(bulge)$). Shown separately are: S0s (red filled symbols), Sa-Sbc spirals (crosses), and Sc and later types (squares). The dashed line shows the location of the Coma cluster ellipticals, taken from Graham & Worley (2008): $\log r_{eff}[\text{kpc}] = 1.137 + 0.217b_n + M_B/10 + 0.5 \log [b_n^{2n} / (n\Gamma(2n)e^{b_n})]$, where $b_n \sim 1.9992n - 0.3271$, for $0.5 < n < 10$; the value of n is expressed as: $n = 10^{-(14.30+M_B)/9.4}$. The continuous lines show the mean values of the data points in one magnitude bins: red (thicker) line is for S0s and blue (thinner) line for Sab-Sbc spirals. (b) the mean effective surface brightness of the bulge ($\langle \mu \rangle_{eff}$) plotted against the absolute brightness of the bulge ($M_K^o(bulge)$).

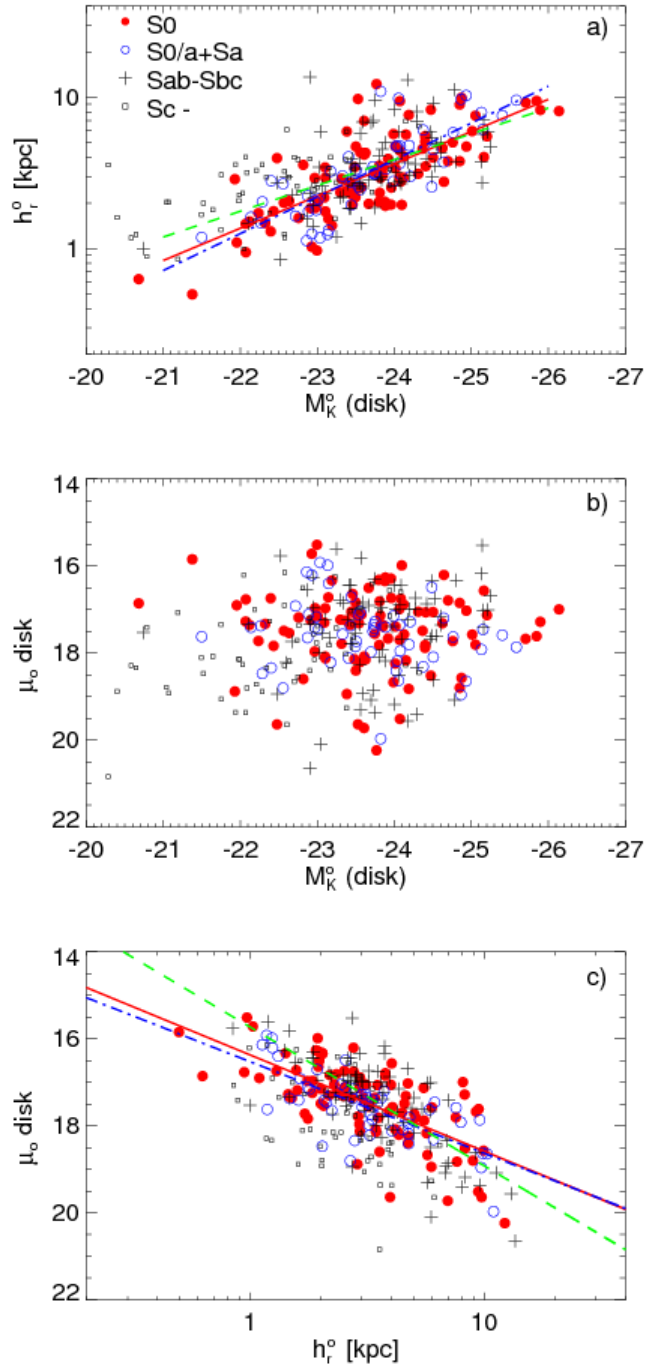


Figure 9. The main parameters of the disk are shown separately for different Hubble type bins: S0s (filled red circles), and S0/a-Sa galaxies (open blue circles) in NIRS0S, and Sab-Sbc (crosses) and Sc and later types (squares) in OSUBSGS. (a) scale length of the disk (h_r^o) vs. disk mass ($M_K^o(disk)$), (b) central surface brightness of the disk (μ_o) vs. disk mass ($M_K^o(disk)$), and (c) central surface brightness of the disk (μ_o) vs. scale length of the disk (h_r^o). The solid, dash-dotted and dashed lines in panels a) and c) indicate the best fits for S0s, S0/a+Sa, and Sab-Sbc galaxies, all having statistically significant rank correlation coefficients.

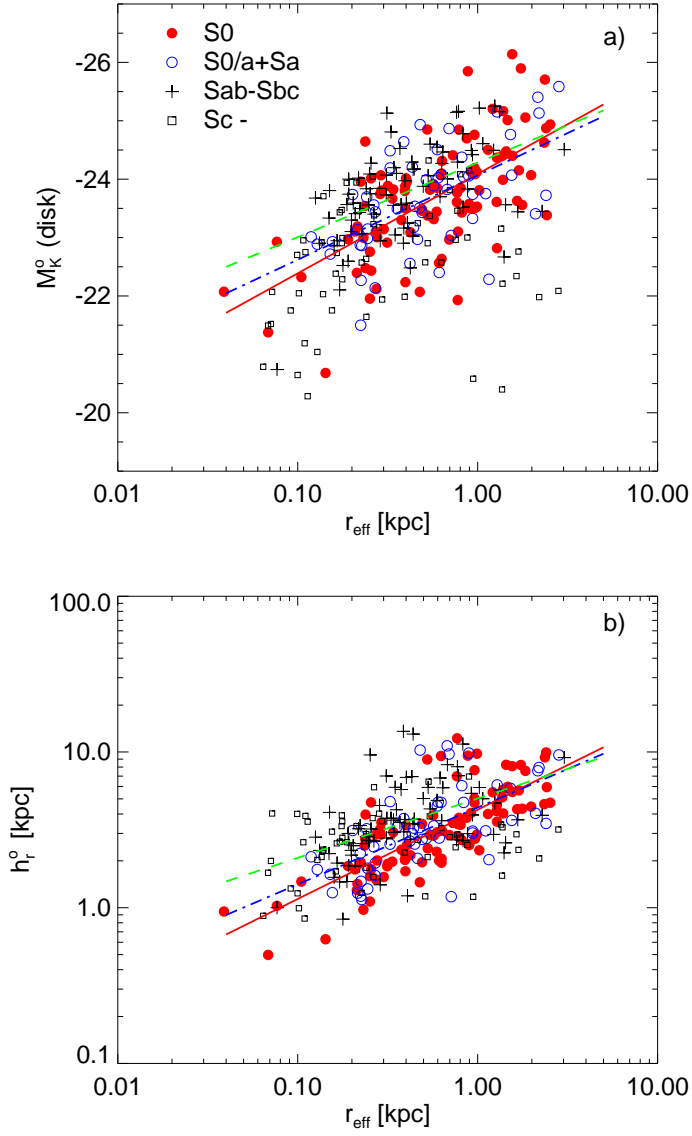


Figure 10. (a) Absolute magnitude of the disk ($M_K^o(\text{disk})$), indicative of its mass, is plotted against the effective radius of the bulge (r_{eff}), shown in different Hubble type bins. The symbols are as in the previous figures, and the lines are the best fits to the data points in different Hubble type bins: S0s (red full line), S0/a-Sa (blue dash-dotted line), Sab-Sbc (green dashed line). (b) Scale length of the disk (h_r^o) plotted against the effective radius of the bulge (r_{eff}). The correlations are significant for all the other bins, except for spirals Sc and later.

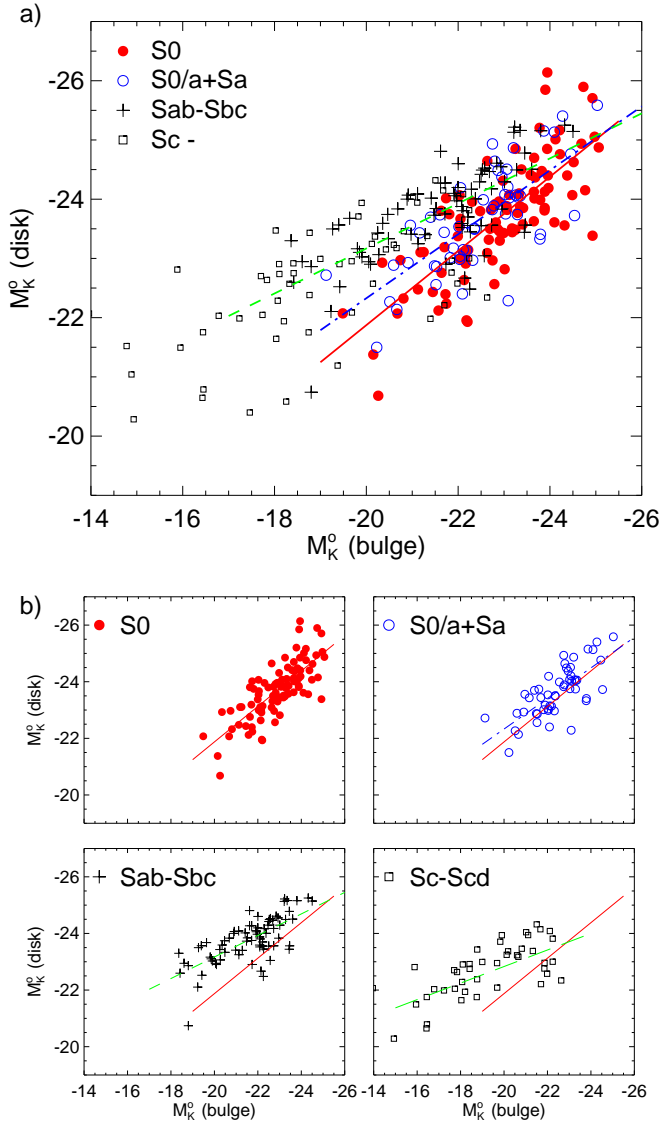


Figure 11. Absolute brightness of the disk ($M_K^o(disk)$) is plotted against the absolute brightness of the bulge ($M_K^o(bulge)$). (a) S0s (red filled circles), S0/a+Sa (open blue circles), Sab-Sbc (crosses) and Sc and later types (squares). Solid, dash-dotted and dashed lines show linear fits for S0s, S0/a+Sa and Sab-Sbc galaxies, respectively, all correlations being statistically significant. The correlation for the latest type galaxies is also statistically significant, but for clarity the fit is not shown. (b) the correlation is shown separately in different Hubble type bins. In the lower panels the solid lines indicate the linear fit for the S0 galaxies.